JOURNAL OF MATERIALS SCIENCE 23 (1988) 1–20

Review
Creep of ceramics
Part 2 *An examination of flow mechanisms*

W. ROGER CANNON
Department of Ceramics, Rutgers University, Piscataway, New Jersey 08854, USA
TERENCE G. LANGDON
Departments of Materials Science and Mechanical Engineering, University of Southern California, Los Angeles, California 90089–1453, USA

This review analyses a wide range of experimental data on the creep of ceramic materials and reveals many similarities with the creep of metals. It is demonstrated that there are two important differences in the creep behaviour of ceramics: (1) there is an enhanced role of diffusion creep, and (2) in the power-law regime, ceramics divide into two categories with stress exponents of ~ 5 and ~ 3, respectively. It is concluded that the behaviour with an exponent of ~ 5 represents fully ductile behaviour as in f c c metals, whereas the behaviour with an exponent of ~ 3 is due to dislocation climb from Bardeen–Herring sources under conditions where there is either a lack of five independent slip systems or, if five independent slip systems are available, a lack of interpenetration of these systems.

1. Introduction

The creep behaviour of ceramic materials is of considerable current interest because of the development of structural ceramics for applications at high temperatures. Part 1 of this review [1] gave a very brief outline of possible creep mechanisms and a detailed compilation, in tabular form, of the various creep data published in the scientific literature on ceramic materials in single crystal, bicrystal and polycrystalline form. In Part 2, the data are analysed and compared for several selected materials, the substructural features are examined, and there is also a direct comparison with the general trends anticipated in metals.

As noted in Part 1 [1], the steady-state creep rate, $\dot{\varepsilon}$, may be expressed in the form

$$\dot{\varepsilon} = \frac{ADG\boldsymbol{b}}{kT}\left(\frac{b}{d}\right)^p\left(\frac{\sigma}{G}\right)^n \quad (1)$$

where D is the appropriate diffusion coefficient, G is the shear modulus, $\boldsymbol{b}$ is the Burgers vector, k is Boltzmann's constant, T is the absolute temperature, d is the grain size, σ is the applied stress, p is the exponent of the inverse grain size, n is the stress exponent, and A is a dimensionless constant. The diffusion coefficient, D, is given by

$$D = D_0 \exp(-Q/RT) \quad (2)$$

where D_0 is a frequency factor, Q is the activation energy for the appropriate diffusion process, and R is the gas constant ($8.31\ \mathrm{J\,mol^{-1}\,K^{-1}}$).

It follows from Equation 1 that a comparison of data may be conveniently achieved by logarithmically plotting the individual datum points in the form $(\dot{\varepsilon}kT/DG\boldsymbol{b})\ (d/\boldsymbol{b})^p$ against σ/G.

A further simplification is possible because, as noted in Part 1 [1], lattice creep mechanisms are based on the intragranular movement of dislocations and, by definition, they require that $p = 0$. Thus, for materials exhibiting intragranular dislocation creep, the data may be logarithmically plotted as $\dot{\varepsilon}kT/DG\boldsymbol{b}$ against σ/G.

In general, the creep behaviour of polycrystalline ceramics falls into two distinct categories. Many ceramics exhibit a stress exponent close to 1 and a value of p which is typically ~ 2 to 3. There are also many ceramics exhibiting a stress exponent of ~ 3 to 5 and creep rates which are independent of grain size so that $p = 0$. These two categories of behaviour are interpreted in terms of boundary creep mechanisms and lattice creep mechanisms, respectively: the various possible creep mechanisms were summarized in Tables I and II of Part 1 [1].

This report is divided into four parts. First, data are collected and plotted graphically for several materials exhibiting a stress exponent close to 1. Second, a similar correlation is presented for several ceramics exhibiting stress exponents of ~ 3 to 5. (It should be noted that an attempt was made to include in these compilations all data exhibiting either $n \simeq 1$ or $n \simeq 3$ to 5 for materials where the diffusion coefficients are known reasonably well. In practice, there are often some difficulties in deciding on the appropriate diffusion coefficients, and these problems, and the relevant creep models, are discussed in detail in each section.) Third, the substructural parameters are presented graphically for several ceramics. Fourth, the creep behaviour of ceramics is compared directly with the established creep behaviour of metals.

0022–2461/88 $03.00 + .12

2. Ceramics exhibiting $n \simeq 1$

2.1. Creep mechanisms

When a ceramic material exhibits a stress exponent close to 1, there is usually also a dependence on grain size so that $p \neq 0$ and the behaviour is attributed to some form of diffusion creep. (An exception to this rule is Harper–Dorn creep where $n = 1$ and $p = 0$. Harper–Dorn creep is of relatively minor importance in ceramics, but the process is considered briefly at the end of this section.) In this creep process, vacancies diffuse from those grain boundaries situated more nearly perpendicular to the tensile axis where the vacancy concentration is above the equilibrium value to those grain boundaries situated more nearly parallel to the tensile axis where the vacancy concentration is below the equilibrium value.

If the vacancies flow through the grains, the process is termed Nabarro–Herring creep [2, 3] and the steady-state creep rate is given by

$$\dot{\varepsilon} = \frac{B_1 \Omega D_1 \sigma}{d^2 kT} \tag{3}$$

where Ω is the atomic volume, D_1 is the coefficient for lattice self-diffusion and B_1 is a constant. The calculated values of B_1 range from ~ 12–40 for different experimental conditions [4] but Herring [3] obtained $B_1 = 13.3$ for polycrystals having complete grain-boundary relaxation tested in uniaxial tension.

Taking $B_1 = 13.3$ and $\Omega = 0.7\boldsymbol{b}^3$, Equation 3 may be expressed in the form of Equation 1 as

$$\dot{\varepsilon} = 9.3 \frac{D_1 G \boldsymbol{b}}{kT} \left(\frac{\boldsymbol{b}}{d}\right)^2 \left(\frac{\sigma}{G}\right) \tag{4}$$

If the vacancies flow along the grain boundaries, the process is termed Coble creep [5] and the steady-state creep rate is given by

$$\dot{\varepsilon} = \frac{150 \Omega \delta D_{gb} \sigma}{\pi d^3 kT} \tag{5}$$

where δ is the effective width of the grain boundary for vacancy diffusion and D_{gb} is the coefficient for grain-boundary diffusion.

Again, taking $\Omega = 0.7\boldsymbol{b}^3$, Equation 5 becomes

$$\dot{\varepsilon} = 33.4 D_{gb} \frac{G\boldsymbol{b}}{kT} \left(\frac{\delta}{\boldsymbol{b}}\right) \left(\frac{\boldsymbol{b}}{d}\right)^3 \left(\frac{\sigma}{G}\right) \tag{6}$$

A comparison of Equations 4 and 6 shows that Coble creep is favoured over Nabarro–Herring creep when the grain size is very small (because the values of p are 3 and 2 for Coble and Nabarro–Herring creep, respectively) and at the lower testing temperatures (because $Q_{gb} < Q_1$, where Q_{gb} and Q_1 are the activation energies for grain-boundary and lattice diffusion, respectively).

In practice, the Nabarro–Herring and Coble creep processes operate independently, so that the rates are additive and the total creep rate is given by

$$\dot{\varepsilon} = 9.3 \frac{D_1 G \boldsymbol{b}}{kT} \left(\frac{\boldsymbol{b}}{d}\right)^2 \left(\frac{\sigma}{G}\right) \left[1 + 3.6 \frac{D_{gb}}{D_1} \left(\frac{\delta}{d}\right)\right] \tag{7}$$

The situation is more complex in ceramics than metals because of the presence of two ionic species. The deformation of ceramic grains results from flow of both the cations and the anions and, in the steady-state condition, the total flux of these two components must be in the stoichiometric ratio. Thus, considering the possibilities of cation and anion diffusion along both lattice and grain-boundary paths, the total diffusion creep rate of a ceramic leads to a modification of Equation 7 given by [6, 7]

$$\dot{\varepsilon} = 9.3 \left(\{(1/\alpha)[D_{c(l)} + 3.6 D_{c(gb)}(\delta_c/d)]\} \Big/ \left\{1 + \left(\frac{\beta}{\alpha}\right) \frac{[D_{c(l)} + 3.6 D_{c(gb)}(\delta_c/d)]}{[D_{a(l)} + 3.6 D_{a(gb)}(\delta_a/d)]}\right\}\right) \times \left(\frac{G\boldsymbol{b}}{kT}\right) \left(\frac{\boldsymbol{b}}{d}\right)^2 \left(\frac{\sigma}{G}\right) \tag{8}$$

where D_c denotes diffusion of the cation, D_a denotes diffusion of the anion, δ_c and δ_a are the effective grain-boundary widths for the cation and anion, respectively, and β and α are the valences of the cation and anion, respectively.

Equation 8 becomes simplified in practice because of the large differences in the values of the individual diffusion coefficients. The various implications of Equation 8 were summarized earlier in tabular form by Evans and Langdon [8] and the overall conclusion is that the observed creep rates are determined by the movement of the slower diffusing species along the faster diffusion path.

As noted earlier, an additional mechanism giving $n = 1$ is Harper–Dorn creep. This process was first identified by Harper and Dorn [9] in creep experiments on pure aluminium, and it was subsequently confirmed in independent experiments on aluminium and on several other metals: a detailed summary of this work is given by Yavari *et al.* [10].

All of the published data for this mechanism indicate a creep rate of the form [10]

$$\dot{\varepsilon} = B_{HD} \frac{D_1 G \boldsymbol{b}}{kT} \left(\frac{\sigma}{G}\right) \tag{9}$$

where B_{HD} is a constant having an experimental value of the order of 10^{-11}.

Equation 9 is reasonably consistent with the climb of edge dislocations under saturated conditions [11]. The latter mechanism gives [12]

$$\dot{\varepsilon} = \frac{2\pi\varrho\boldsymbol{b}^2}{\ln(1/\varrho^{1/2}\boldsymbol{b})} \frac{D_1 G \boldsymbol{b}}{kT} \left(\frac{\sigma}{G}\right) \tag{10}$$

where ϱ is the dislocation density. Taking the experimentally measured value of $\varrho \simeq 5 \times 10^3 \text{cm}^{-2}$, Equation 10 reduces to Equation 9 with $B_{HD} \simeq 2 \times 10^{-12}$.

Inspection of Equation 9 shows that Harper–Dorn creep predicts $n = 1$ and no dependence on grain size so that $p = 0$. Thus, Harper–Dorn creep becomes important only when the grain size is large (typically $> 400\,\mu\text{m}$ [11]).

Although it is reasonable to assume that Harper–Dorn creep occurs in non-metallic materials, there is very little experimental evidence for this mechanism because most of the experiments have been performed

TABLE I Values of the material parameters

Material	D ($cm^2\ sec^{-1}$)*	G_0 (MPa)	ΔG ($MPa\ K^{-1}$)	b (cm)	References	
					D	G
Al_2O_3	$D_l(O^{2-}) = 2 \times 10^3 \exp(-635000/RT)$ $D_l(Al^{3+}) = 28 \exp(-476000/RT)$	1.71×10^5	23.4	4.75×10^{-8}	[18] [20]	[19]
MgO	$D_l(O^{2-}) = 2.5 \times 10^{-6} \exp(-261000/RT)$ $D_l(Mg^{2+}) = 2.49 \times 10^{-1} \exp(-330000/RT)$	1.387×10^5	26.2	2.98×10^{-8}	[21] [23]	[22]
BeO	$D_l(O^{2-}) = 2.7 \times 10^{-5} \exp(-284000/RT)$ $D_l(Be^{2+}) = 1.5 \exp(-384000/RT)$	1.86×10^5	20	2.7×10^{-8}	[24] [26]	[25]
SiC	$D_l(Si^{4+})(\alpha) = 2.6 \times 10^8 \exp(-840000/RT)$ $D_l(Si^{4+})(\beta) = 8.4 \times 10^7 \exp(-911000/RT)$	1.6×10^5	23	3×10^{-8}	[27] [29]	[28]
Si_3N_4	$D_l(N^{3-})(\alpha) = 1.2 \times 10^{-12} \exp(-233000/RT)$†	1.3×10^5‡		3×10^{-8}§	[30]	[31]
UO_2	$D_l(U^{4+}) = 6.8 \times 10^{-5} \exp(-410000/RT)$	8.9×10^4	21	3.87×10^{-8}	[32]	[33]
ThO_2	$D_l(Th^{4+}) = 1.25 \times 10^{-7} \exp(-245000/RT)$	9.0×10^4	19	3.96×10^{-8}	[34]	[35, 36]
NaCl	$D_l(Cl^-) = 1.2 \times 10^2 \exp(-214000/RT)$	1.79×10^4	9.6	3.99×10^{-8}	[37]	[38]
LiF	$D_l(F^-) = 64 \exp(-212000/RT)$	5.52×10^4	33.2	2.85×10^{-8}	[39]	[38]
KCl	$D_l(Cl^-) = 2.1 \exp(-189000/RT)$	1.225×10^4	6.57	4.45×10^{-8}	[37]	[38]
UC	$D_l(U^{4+}) = 7.5 \times 10^{-5} \exp(-339000/RT)$	2.058×10^6	16.1	3.51×10^{-8}	[40]	[41]
Fe_2O_3	$D_l(O^{2-}) = 2.0 \exp(-326000/RT)$	9.28×10^4	6.0	5.03×10^{-8}	[42]	[43, 44]
ZrO_2	$D_l(Zr^{4+}) = 3.5 \times 10^{-2} \exp(-387000/RT)$	1.54×10^5	35.2	2.57×10^{-8}	[45]	[46]

*Activation energies in $J\ mol^{-1}$ ($R = 8.31\ J\ mol^{-1}\ K^{-1}$).
†Measured by isotope exchange assuming rapid boundary diffusion of N.
‡Value of G at test temperature of 1748 K.
§Estimated from $b = (\Omega/0.7)^{1/3}$.

outside of the Harper–Dorn range using polycrystalline samples with very small grain sizes. There is evidence for Harper–Dorn creep in two sets of experimental data using non-metallic single crystals, on $KZnF_3$ [13] and NaCl [14], respectively, and it is also possible to interpret experimental data on single crystal and polycrystalline CaO [15] in terms of the Harper–Dorn process [16]. However, in view of the paucity of data on Harper–Dorn creep in ceramics, this mechanism is not considered in the following section.

2.2. Correlation between various materials

It was assumed in early work on ceramics that, if lattice diffusion controls the creep rate, the diffusion of the slower moving species through the lattice is rate-controlling (usually the anion) and the diffusion of the faster moving species through the lattice may be neglected (usually the cation). However, it was first pointed out by Paladino and Coble [17] that the creep of Al_2O_3 is controlled by diffusion of the faster moving aluminium cation. This observation was explained by noting that the oxygen anion diffuses extremely rapidly along the grain boundaries, and it was suggested that the grain-boundary diffusion of oxygen was faster than either the boundary or lattice diffusion of aluminium. More recently, similar behaviour has been ascribed to some other materials, e.g. MgO, BeO, etc.

A consequence of this effect is that it cannot be assumed, *a priori*, that either anion or cation diffusion controls the creep rate, and thus there is a difficulty in correlating the data for different materials because of uncertainties in the precise values of the diffusion coefficients.

In this report, the data are graphically presented for the materials exhibiting $n \simeq 1$, and in each case the diffusion coefficient was selected to provide the best fit with the theoretical model. In most cases, the best fit was obtained using diffusion data for the more rapidly diffusing species through the crystal lattice.

Figs 1 to 4 show plots for several materials in the form $(\dot{\varepsilon}kT/DGb)\,(d/b)^2$ against σ/G. These plots follow from Equation 4, and the broken lines with $n = 1$ are the predictions for Nabarro–Herring creep using $B_1 = 13.3$ in Equation 3. Figs 1 to 4 cover all of the data from Part 1 [1] where sufficient results are available and it seems that Nabarro–Herring creep is rate-controlling; the plots exclude the limited experimental data giving $n \simeq 1$ and $p \simeq 3$ because this indicates a dominance by Coble diffusion creep and there are too few measurements of the relevant grain-boundary diffusion coefficients for any meaningful comparisons.

Table I lists the various values, and appropriate references, for D, G and b for each material documented in Figs 1 to 4. The shear modulus, G, was estimated at the appropriate temperature using the expression

$$G = G_0 - (\Delta G)\,T \qquad (11)$$

where G_0 is the value of the shear modulus obtained by linear extrapolation from high temperatures to absolute zero and ΔG is the variation in shear modulus per degree Kelvin.

Fig. 1 shows data for Al_2O_3 containing no additives [47–49] using $D = D_l(Al^{3+})$, Fig. 2 shows data for Al_2O_3 containing various levels of MgO additions [48, 50–52] using $D = D_l(Al^{3+})$, Fig. 3 shows data for MgO [53], BeO [54, 55], α-SiC [56] and Si_3N_4 [57] using

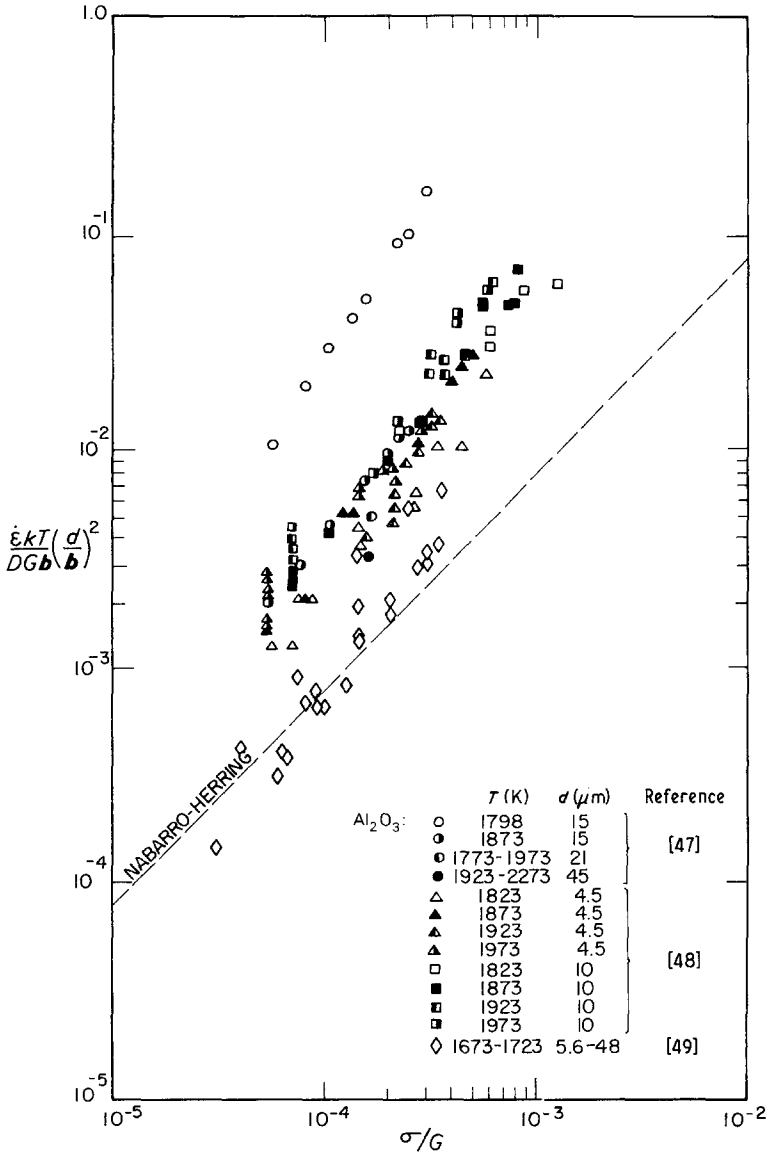

Figure 1 Normalized creep rate plotted against normalized stress for Nabarro–Herring creep in Al_2O_3 containing no additives [47–49].

values for D of D_l (Mg^{2+}), D_l (Be^{2+}), D_l (Si^{4+}) (α) and D_l (N^{3-}) (α), respectively, and Fig. 4 shows data for UO_2 [58–63] and ThO_2 [58] using D_l (U^{4+}) and D_l (Th^{4+}), respectively.

Inspection of Figs 1 to 4 shows that the experimental datum points lie close to a slope of $n = 1$ for any selected material and testing condition, and the experimental creep rates generally agree with the predicted rate for Nabarro–Herring creep to within about one or two orders of magnitude. Three specific reasons may be cited for the discrepancies between the predicted rates and the experimental rates. First, the measured creep rates tend to vary with the mode of testing. In Fig. 2 for Al_2O_3 doped with MgO, for example, the tensile results by Davies [51] are faster than the bending results of Folweiler [50] and Heuer *et al.* [48], and both of these sets are faster than the results in compression by Cannon and Sherby [52]. In fact, the latter results are in very close agreement with the theoretical prediction. Second, the diffusion coefficients, and therefore the creep rates, vary with the level of impurities, and it is doubtful whether the creep rates are ever strictly controlled by intrinsic diffusion. For example, Fig. 1 reveals large variations in the data for Al_2O_3 where no impurities were intentionally added, although each individual result gives a stress exponent close to 1. Third, discrepancies arise when the compositions deviate from stoichiometry as, for example, in UO_2. Although Fig. 4 was constructed using data from materials which were judged to be close to stoichiometric, the large variations in the datum points for the different materials are probably due to small deviations from stoichiometry.

The results for Si_3N_4 and α-SiC in Fig. 3 are of particular interest.

Many creep studies have been reported on a variety of hot-pressed, sintered and reaction-bonded silicon nitride materials. In most cases, the experimental creep rates depend upon the presence of a glassy phase at the grain boundaries and/or triple points so that a comparison with Nabarro–Herring diffusion creep is meaningless. However, it appears that the creep data of Seltzer [57] on reaction-bonded NC350 silicon nitride may be ascribed to the Nabarro–Herring or Coble mechanisms. The NC350 material contained a low impurity level and probably little or no glassy grain-boundary phase, and it exhibited the lowest creep rate of any silicon nitride tested to date. Internal oxidation was apparently prevented in this material by a fine pore structure. As indicated in Fig. 3, the creep results on NC350 Si_3N_4 give a stress exponent of 1 and the rates agree with the Nabarro–Herring mechanism

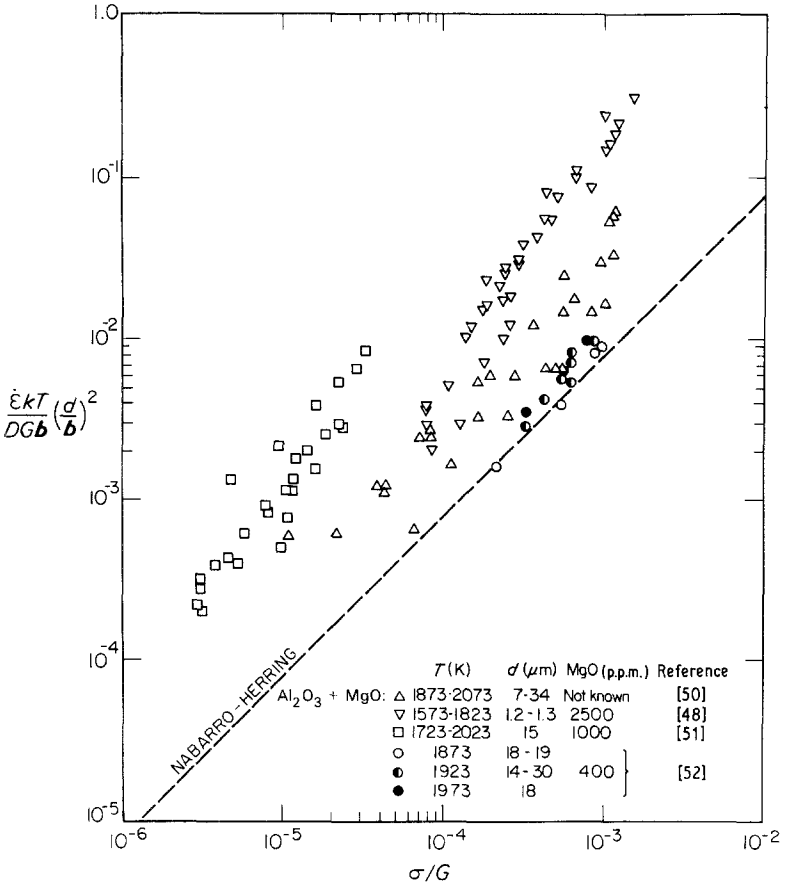

Figure 2 Normalized creep rate plotted against normalized stress for Nabarro–Herring creep in Al_2O_3 containing various levels of MgO additions [48, 50–52].

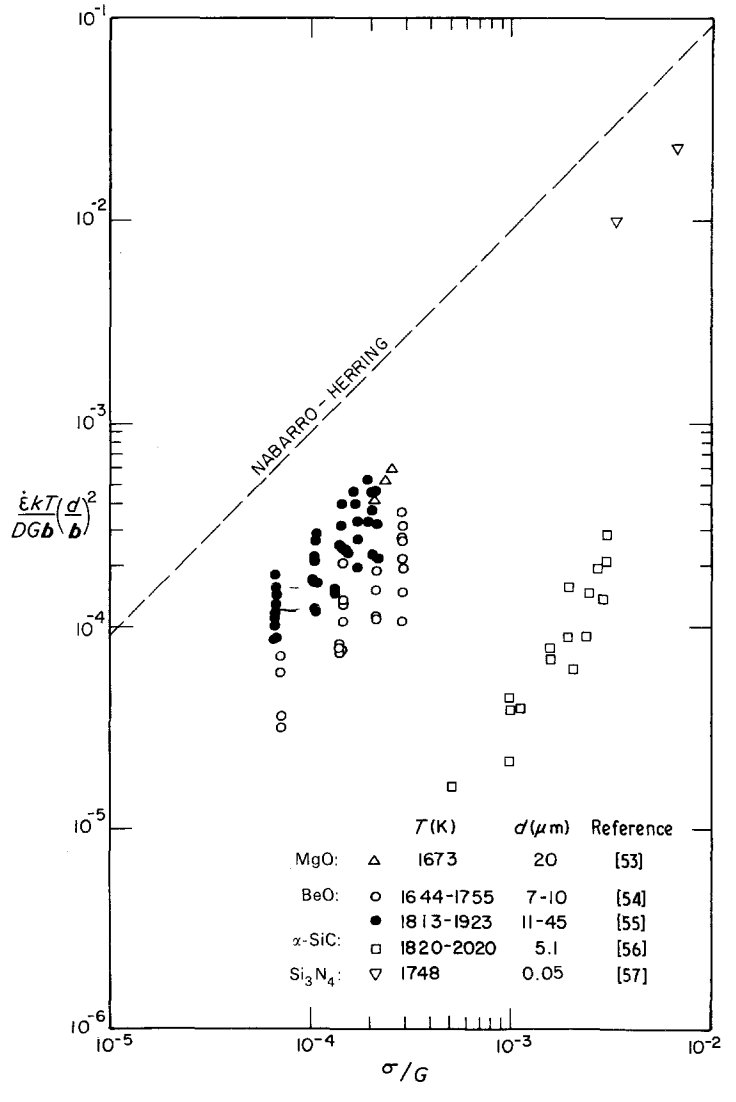

Figure 3 Normalized creep rate plotted against normalized stress for Nabarro–Herring creep in (△) MgO [53], (○, ●) BeO [54, 55], (□) α-SiC [56] and (▽) Si_3N_4 [57].

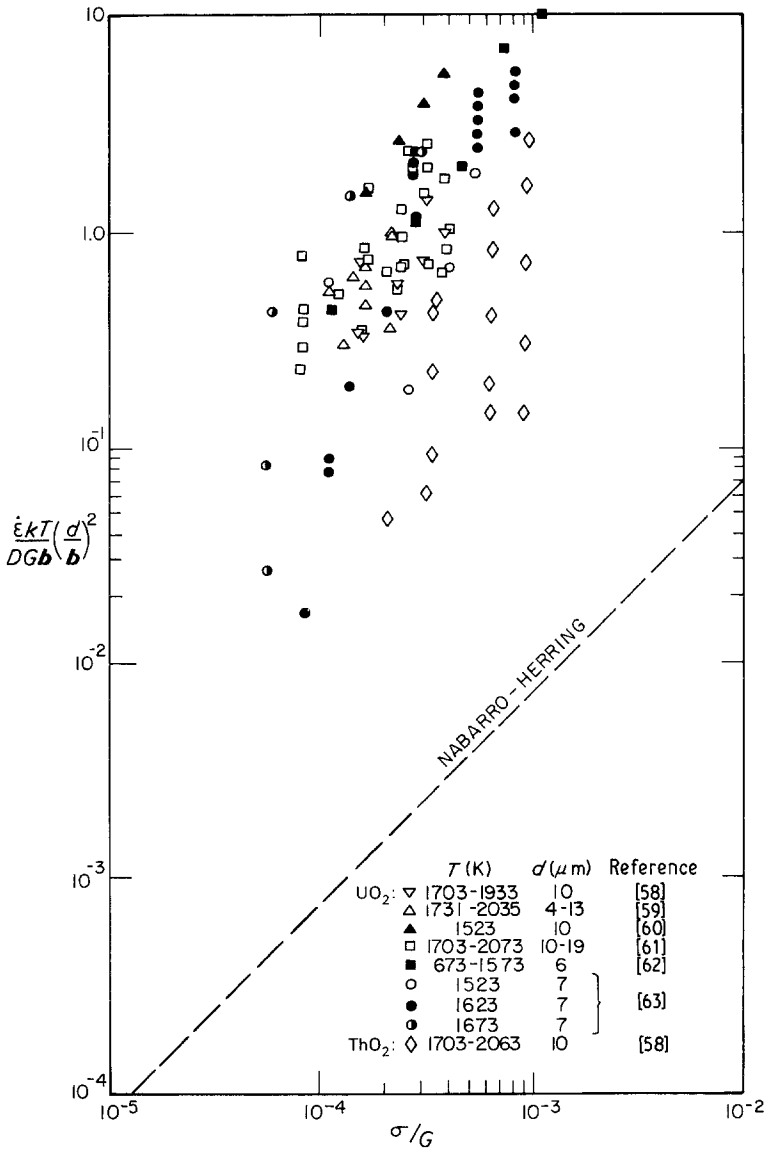

Figure 4 Normalized creep rate plotted against normalized stress for Nabarro–Herring creep in UO_2 [58–63] and ThO_2 [58].

to within a factor of about four times. It was assumed that nitrogen diffusion was rate-controlling and diffusion was determined by gas–solid isotope exchange. The grain size of the reaction bonded NC350 silicon nitride was not known but typical values vary between 0.04 and 0.05 μm. A value of 0.05 μm was used here.

For α-SiC, the material had a nearly equiaxed grain size of $\sim 5.1\,\mu$m and apparently no grain-boundary glassy phase [56]. The correlation in Fig. 3 was achieved using the slowest moving species, D_l (Si^{4+}) (α), as rate-controlling. In practice, the experimental creep rates may be affected by boron–carbon additions, but this should make the rates faster, rather than slower, than the predicted values.

3. Ceramics exhibiting $n \sim 3$ to 5

3.1. Creep mechanisms

Many ceramic materials exhibit stress exponents of ~ 3 to 5 and creep rates which are independent of the grain size. As noted in Part 1 [1], this behaviour is attributed to the intragranular motion of dislocations. Many theoretical creep mechanisms have been developed to explain these high stress exponents and a detailed tabulation was presented in Part 1. For the present purpose, it is sufficient simply to summarize the important characteristics of those mechanisms which appear to be of major importance in the creep of ceramics.

It is well established that many metals exhibit a stress exponent close to 5. This behaviour is usually interpreted in terms of the glide and climb of intragranular dislocations, where the dislocations pile-up and the climb process is rate-controlling. The steady-state creep rate for this mechanism is given by [64]

$$\dot{\varepsilon} = \frac{B_2 \Omega D_l \sigma^{4.5}}{G^{3.5} M^{0.5} \boldsymbol{b}^{3.5} kT} \tag{12}$$

where M is the concentration of active dislocation sources and B_2 is a constant.

Assuming that the piled-up arrays of dislocations decompose into groups of dislocation dipoles [65], the value of B_2 is in the range 0.015 to 0.33 [66]. Thus, taking $B_2 = 0.2$, Equation 12 reduces to

$$\dot{\varepsilon} = \frac{0.14}{\boldsymbol{b}^{1.5} M^{0.5}} \left(\frac{D_l G \boldsymbol{b}}{kT}\right)\left(\frac{\sigma}{G}\right)^{4.5} \tag{13}$$

Equation 13 includes the lattice diffusivity, D_l, and it assumes that the diffusion involved in the climb process occurs exclusively through the crystalline lattice. This is true at temperatures above about $0.5\,T_m$, where T_m is the melting temperature in degrees Kelvin, but it breaks down at lower temperatures

where pipe diffusion along the dislocation cores becomes dominant. (The advent of pipe diffusion leads to a decrease in the activation energy for creep at lower testing temperatures; see, for example, results on polycrystalline NaCl [67, 68].) To avoid these difficulties, all of the experimental data correlated in Section 3.2 for ceramics exhibiting $n \simeq 5$ were obtained at temperatures above 0.6 T_m, and the appropriate diffusion coefficient was taken for the slower moving species through the lattice.

Two mechanisms should be considered in examining the creep behaviour of ceramic materials where $n \simeq 3$.

First, there is much evidence for a stress exponent close to 3 in many metallic solid solution alloys, and this is usually interpreted in terms of a glide and climb process controlled by glide due to the viscous dragging of solute atom atmospheres around the dislocations. The steady-state creep rate for this process is given by [69, 70]

$$\dot{\varepsilon} = \frac{\pi(1-\mu)kT\tilde{D}\sigma^3}{6e^2c\boldsymbol{b}^5G^4} \quad (14)$$

where μ is Poisson's ratio, $\tilde{D}$ is the solute interdiffusion coefficient, e is the solute–solvent size difference and c is the concentration of solute.

Taking $\mu = 0.34$, Equation 14 reduces to

$$\dot{\varepsilon} = \frac{0.35}{e^2c}\left(\frac{kT}{G\boldsymbol{b}^3}\right)^2\left(\frac{\tilde{D}G\boldsymbol{b}}{kT}\right)\left(\frac{\sigma}{G}\right)^3 \quad (15)$$

A more recent model for this process, based on a homogeneous distribution of edge dislocations, also leads to Equation 15 but with the numerical factor of 0.35 replaced by 0.125 [71].

Equation 15 was derived for the drag of solute atom atmospheres. However, most ceramics exhibiting $n \simeq 3$ contain no solute, and it is therefore necessary to invoke either charged vacancy drag or charged impurity drag due to the higher polarizability of the constituent ions in these materials [72]. A problem associated with charged vacancy drag is that, if vacancy diffusion is rate-controlling, $\tilde{D}$ in Equation 14 is replaced by the vacancy diffusion coefficient, D_v, and because $D_v = D_l/N_v$, where N_v is the vacancy concentration, and c is now equal to N_v in Equation 14, the steady-state creep rate is proportional to D_l/N_v^2. Because N_v is very small in most ceramics, this necessitates a strong interaction force. Thus, it is more likely that drag is controlled by impurity ion diffusion, but the relevant impurity diffusion coefficients are not generally known and it was therefore not possible to include this mechanism in the correlation of creep data.

Second, if creep is controlled by the climb of dislocations from Bardeen–Herring sources, the creep rate is given by [73]

$$\dot{\varepsilon} = \frac{B_3\pi\Omega D_l\sigma^3}{G^2\boldsymbol{b}^2kT} \quad (16)$$

where B_3 is a constant having a value of ~ 0.1 [74].

Equation 16 reduces to

$$\dot{\varepsilon} = 0.22\frac{D_lG\boldsymbol{b}}{kT}\left(\frac{\sigma}{G}\right)^3 \quad (17)$$

where D_l is for the slower moving species in the lattice. Because all of the various terms in Equation 17 are known, the theoretically predicted creep rate may be included in a direct comparison with the experimental data. This comparison is contained in the following section.

3.2. Correlation between various materials

Figs 5 to 9 show a detailed compilation of creep data for ceramic materials exhibiting stress exponents of ~ 3–5. Figs 5 and 6 are for materials where n is close to 5 and Figs 7 to 9 are for materials where n is close to 3. All of the datum points are plotted in the form $\dot{\varepsilon}kT/DG\boldsymbol{b}$ against σ/G, with D taken as the lattice diffusion coefficient for the slower moving species. As previously, Table I lists the relevant data for D, G and $\boldsymbol{b}$.

For $n \simeq 5$, Fig. 5 shows data for NaCl [67], LiF [75], KCl [76], UC [77], and reaction-sintered (RS) SiC [78] using values for D of D_l (Cl^-), D_l (F^-), D_l (Cl^-), D_l (U^{4+}) and D_l (Si^{4+}) (α), respectively, and Fig. 6 shows data for UO_2 [58, 60, 61, 63] and ThO_2 [58] using D_l (U^{4+}) and D_l (Th^{4+}), respectively. For $n \simeq 3$, Fig. 7 shows data for Al_2O_3 [47, 52, 79, 80] and Fe_2O_3 [81] using D_l (O^{2-}) for both materials, Fig. 8 shows data for MgO [49, 82, 83] and BeO [84] using D_l (O^{2-}) and chemically vapour deposited (CVD) SiC [85] using D_l (Si^{4+}) (β), and Fig. 9 shows data for ZrO_2 containing 10% Y_2O_3 [86] using D_l (Zr^{4+}). (For the CVD–SiC in Fig. 8, it was reported that there was a β to α ratio of approximately 60 : 40 for both the as-deposited material and the annealed and crept samples [85]. Thus, D_l (Si^{4+}) was taken for the dominant cubic β-SiC phase. By contrast, the RS-SiC in Fig. 5 was reported as almost totally α-SiC [78] so that D_l (Si^{4+}) was taken for the α-SiC phase. ZrO_2 is an unusual oxide because cation diffusion is slower than anion diffusion [45].

Inspection of Fig. 5 shows very good agreement between the creep data of several alkali halides. The lack of any dependence on grain size in the $n \simeq 5$ region is demonstrated by the similar datum points obtained on NaCl [67] and LiF [75] using samples having grain sizes differing by more than an order of magnitude. The agreement is less satisfactory for UO_2 shown in Fig. 6 and the stress exponent varies from ~ 4 to ~ 6 in different investigations. The scatter in the UO_2 data is probably due to variations in the degree of stoichiometry.

As noted earlier, a stress exponent close to 5 suggests that dislocation climb is the rate-controlling process. However, no attempt was made to compare the experimental data with the predictions of Equation 13 because there are uncertainties in the value of M and, in addition, there is evidence that Equation 13 should be modified to incorporate a dependence on the stacking-fault energy of the material, Γ. Experimental data on several fcc metals show that the measured creep rates are proportional to $(\Gamma/G\boldsymbol{b})^3$ [70], and this proportionality has been used to make reasonable estimates of the values of Γ in the alkali halides [87].

Figs 7 to 9 include broken lines showing the

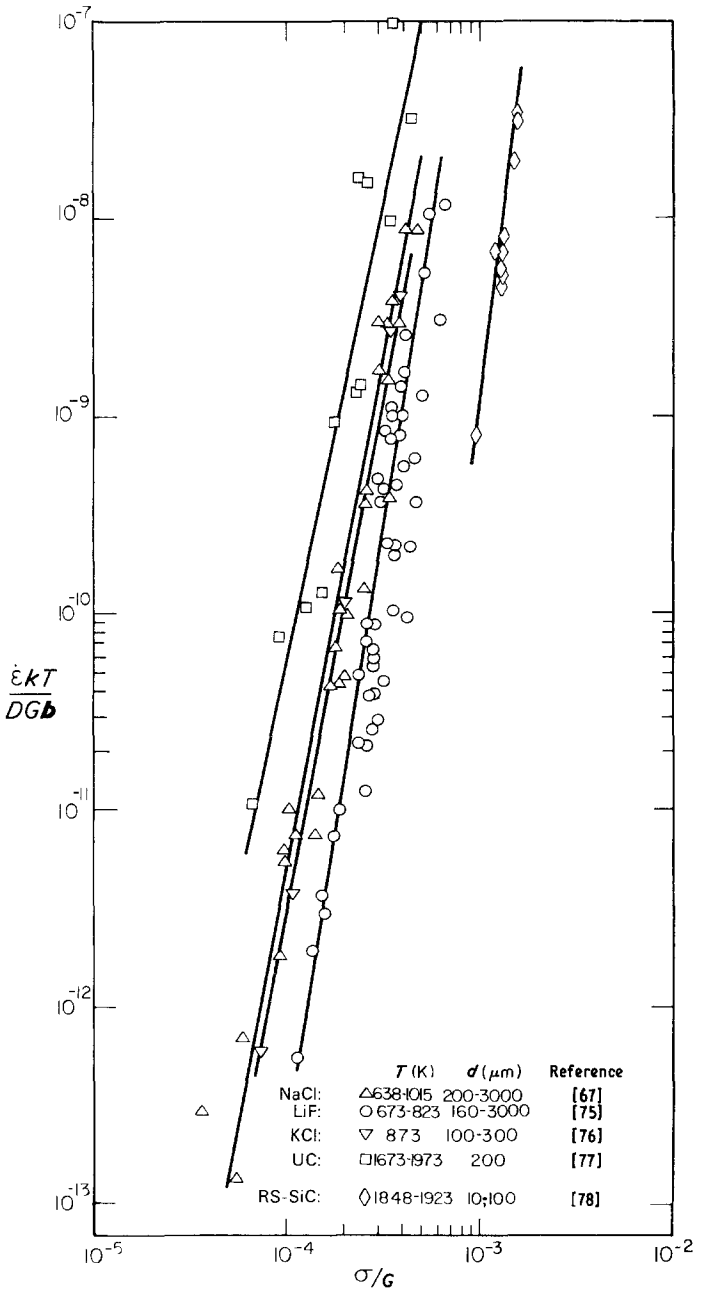

Figure 5 Normalized creep rate plotted against normalized stress for power-law creep in (△) NaCl [67], (○) LiF [75], (▽) KCl [76], (□) UC [77] and (◇) reaction-sintered (RS) SiC [78].

prediction of Equation 17 for dislocations climb from Bardeen–Herring sources. The agreement between the theoretical predictions and the experimental data is excellent for BeO and CVD-SiC in Fig. 8 and ZrO_2 in Fig. 9, and it is generally within an order of magnitude for the other materials.

Fig. 7 includes creep data for Al_2O_3 single crystals with a 0° orientation (the 0° crystals have a stress axis perpendicular to the (0 0 0 1) basal plane) where basal and prismatic slip are suppressed [88]. Although pyramidal slip is possible in this single crystal configuration, there was no experimental evidence for pyramidal slip and, as shown in Fig. 7, there is excellent agreement with the predictions of dislocation climb from Bardeen–Herring sources. The higher creep rates observed in the polycrystalline Al_2O_3 in Fig. 7, and the scatter between the various sets of data, may be due to differences in the impurity levels of the different samples: information on the individual impurity levels was contained in Table AIII of Part 1 [1].

Fig. 10 schematically summarizes the data for the $n \simeq 5$ and $n \simeq 3$ materials. Although the two sets of results are fairly similar in magnitude, the creep data exhibiting $n \simeq 3$ tend to fall below the data exhibiting $n \simeq 5$. This trend is interesting because the climb and glide processes associated with the glide and subsequent climb of dislocations, as represented by Equations 13 and 15, are sequential in nature such that the slower of the two processes is rate-controlling. This means that, for these two processes, there is an anticipated transition from $n \simeq 5$ at the lower stresses to $n \simeq 3$ at the higher stresses, as seen, for example, in metallic solid solution alloys [89]. This anticipated trend is contrary to Fig. 10 where many of the results showing $n \simeq 5$ lie at normalized strain rates which are faster than those associated with $n \simeq 3$.

This observation provides additional support negating the possibility of control by viscous glide and Equation 15 in these ceramics. Conversely, it provides further support for dislocation climb from Bardeen–Herring sources through Equation 17, because additional slip systems are necessary for a general glide–climb process and $n \simeq 5$ behaviour, and these

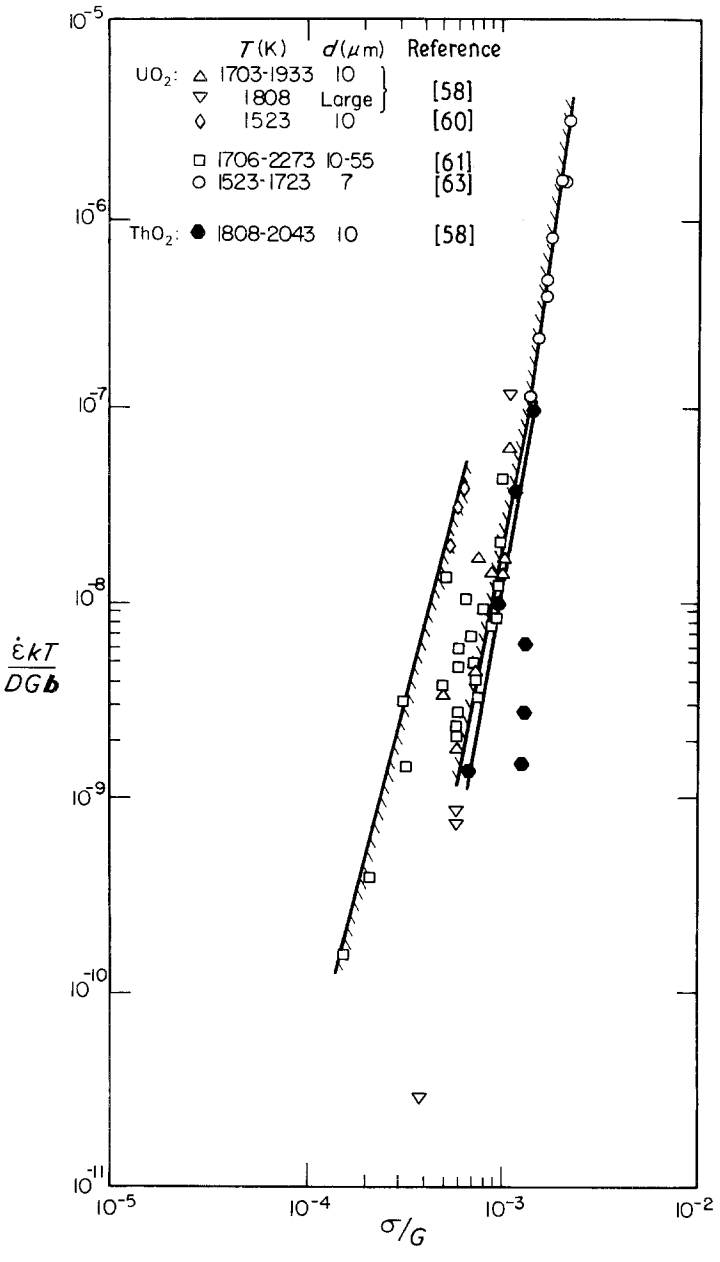

Figure 6 Normalized creep rate plotted against normalized stress for power-law creep in UO_2 [58, 60, 61, 63] and ThO_2 [58].

additional systems do not occur in the 0° Al_2O_3 single crystals [88] in Fig. 7 and they are less likely in the polycrystalline materials at the lower stresses.

4. Substructural characteristics

4.1. Subgrain size

When metals deform by power-law creep with $n \simeq 5$, the grains become divided into subgrains and the subgrain boundaries have very small angles of misorientation (typically $< 2°$). A detailed analysis of the published data for metals has established that the average subgrain size, λ, is related inversely to the applied stress [90]. Measurements show that the normalized subgrain size, $\lambda/\boldsymbol{b}$, is given by

$$\frac{\lambda}{\boldsymbol{b}} = \zeta\left(\frac{\sigma}{G}\right)^{-1} \tag{18}$$

where ζ is a constant having a value close to 20 for all metals.

To check the validity of Equation 18 for ceramics, Fig. 11 logarithmically plots $\lambda/\boldsymbol{b}$ against σ/G for AgCl [91], LiF [92, 93], LiF containing 690 p.p.m. Mg [92], $(Mg, Fe)_2SiO_4$ [94, 95], MgO [96], NaCl [97–99], NaCl single crystals containing various doping levels of calcium [97] and polycrystalline NaCl [67]. Where appropriate, Table I was used to provide the relevant values of $\boldsymbol{b}$ and the shear modulus, G, at the testing temperature; for AgCl, $\boldsymbol{b} = 3.92 \times 10^{-8}$ cm and G was estimated as 7.6×10^3 MPa at the testing temperature of 581 K from measurements of the elastic constants [100]; for $(Mg, Fe)_2SiO_4$, $\boldsymbol{b}$ was taken as 4.79×10^{-8} cm and the value of G was already incorporated in the experimental report of Raleigh and Kirby [94] using published elasticity data [44].

Each line in Fig. 11 is drawn through a single set of datum points with a slope of -1. Although there is some scatter in the individual datum points, there is excellent agreement with the form of Equation 18. Most of the data lie within a factor of two of the mean, except for LiF where the points lie within a factor of four. Using Equation 18, the value of ζ is of the order of 20 to 30 for ceramics, and this value is very similar to, but slightly higher than, the value of 20 for metals. The small difference in the apparent values of ζ for ceramics and metals is not significant because the precise value obtained for any material depends upon

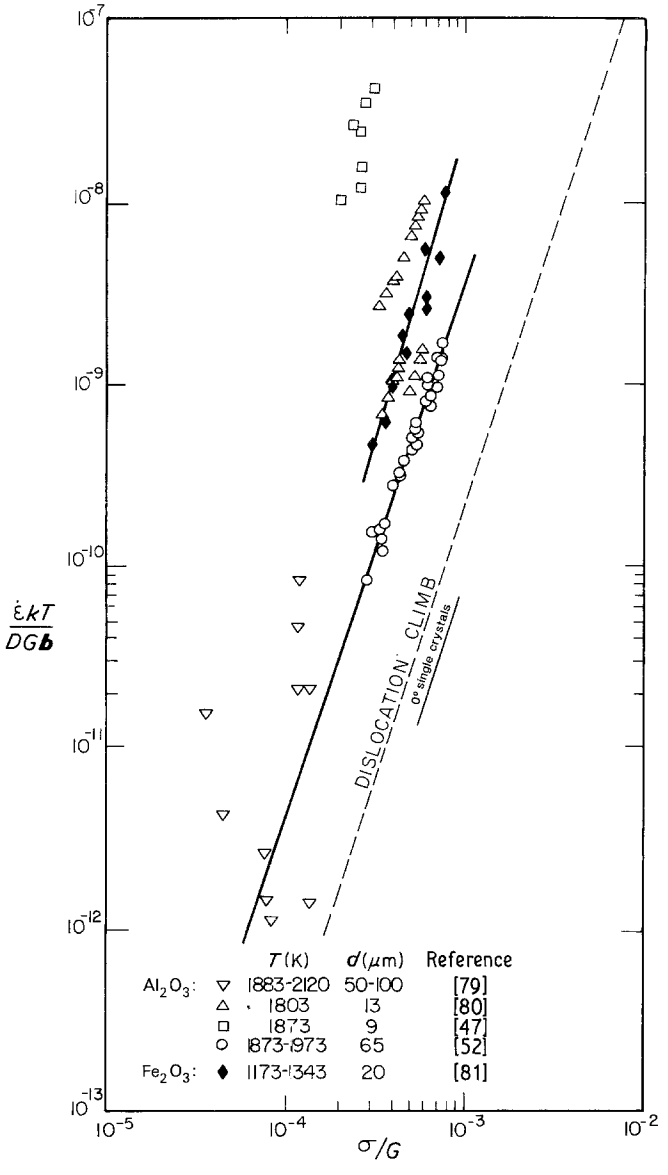

Figure 7 Normalized creep rate plotted against normalized stress for power-law creep in Al_2O_3 [47, 52, 79, 80] and Fe_2O_3 [81]: the short line is for Al_2O_3 single crystals in 0° orientation [88].

the experimental procedure. For example, the data in Fig. 11 for AgCl by Pontikis and Poirier [91] give $\zeta \simeq 23$, whereas an earlier investigation on the same material by the same authors gave $\zeta \simeq 44$ [101]. This difference was ascribed by Pontikis and Poirier [91] to an improvement in the experimental procedure: whereas the datum points shown in Fig. 11 were obtained by using etch pitting to reveal the subgrain boundaries [91], the earlier results used electron imaging to reveal differences in the subgrain orientations [101].

There are three additional observations relating to Fig. 11.

First, it is apparent that a subgrain structure is formed not only in materials exhibiting $n \simeq 5$ such as LiF and NaCl (as in Fig. 5) but also in MgO where $n \simeq 3$ (as in Fig. 8). Furthermore, the observation of subgrain formation in single crystal MgO by Hüther and Reppich [96], as documented in Fig. 11, is supported by similar qualitative reports of subgrain formation in polycrystalline MgO by Bilde-Sörensen [102] and Hurm and Escaig [103]. Thus, unlike metals, a subgrain structure is established in ceramics exhibiting both $n \simeq 5$ *and* $n \simeq 3$.

Second, Fig. 11 contains two points for the orthorhombic mineral olivine, $(Mg, Fe)_2SiO_4$, using the data of Raleigh and Kirby [94] as subsequently amended by Green and Radcliffe [95, 104] through observations of a finer substructure. Evidence from solar-meteoritic atomic abundances and other geophysical data suggests that olivine comprises of the order of 57% of the Earth's upper mantle [105], and it is therefore interesting to note that the two points for olivine in Fig. 11 are in excellent agreement with the data for the alkali halides and MgO at lower stress levels. In addition, the data for ceramics in Fig. 11 are consistent with measurements of λ and stress estimates in naturally deformed rocks [106]. Although this agreement appears to support the use of subgrain measurements as an indirect indicator of tectonic stresses in geological materials [107], it is necessary to exercise caution because of the possibility of at least some subgrain stability when the stress level is reduced [108]. Evidence for subgrain stability following stress reductions is provided by laboratory experiments on AgCl [91] and olivine [109].

Third, using an isolated observation of the subgrain size in deformed quartz rocks [110], White [111] estimated a value of $\zeta \simeq 25$ for minerals. This value is in excellent agreement with the data in Fig. 11, thereby

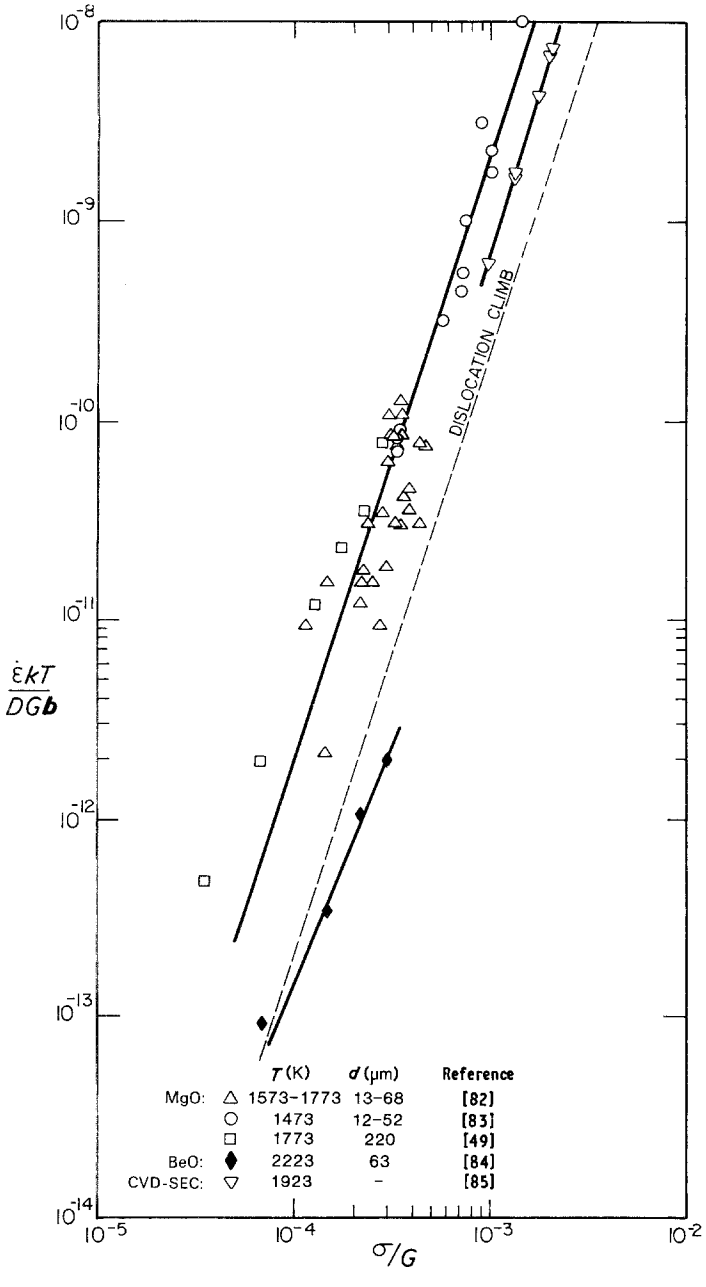

Figure 8 Normalized creep rate plotted against normalized stress for power-law creep in MgO [49, 82, 83], BeO [84] and chemically vapour deposited (CVD) SiC [85].

further confirming the close similarities in subgrain structures between ceramics, metals and minerals.

4.2. Dislocation density within the subgrains

In metals, a detailed analysis shows that the density of dislocations contained within the subgrains, ϱ, varies with σ^2 [90]. The normalized dislocation density, $b\varrho^{1/2}$, may be expressed as

$$b\varrho^{1/2} = \psi\left(\frac{\sigma}{G}\right) \tag{19}$$

where ψ is a constant having a value close to unity for all metals.

To check the validity of Equation 19 for ceramics, Fig. 12 logarithmically plots $b\varrho^{1/2}$ against σ/G for LiF [92], LiF containing 690 p.p.m. Mg [92], MgO [96, 112, 113], NaCl [98] and NaCl containing 1300 p.p.m. Ca [97]. The experimental values of ϱ were taken from both etch pit studies (ϱ_{etch}) and transmission electron microscopy (ϱ_{TEM}), and Fig. 12 was constructed by making the reasonable assumption of $\varrho \simeq \varrho_{TEM} \simeq 2\varrho_{etch}$. The lines in Fig. 12 are drawn through single sets of datum points with a slope of 1.

Although there are only a limited number of measurements of ϱ in ceramics, it is apparent from Fig. 12 that all of the measurements agree with Equation 19 and $\psi = 1$ to within a factor of two. Thus, the agreement between metals and ceramics is excellent.

A similar relationship has been reported also for minerals, with values of ψ of ~ 3 for olivine [114] and ~ 2 for calcite [115].

4.3. Measurements of grain-boundary sliding

Grain-boundary sliding refers to the movement of one grain over an adjacent grain under the action of an applied stress during high-temperature creep. Although the precise atomistic mechanism leading to sliding is not fully understood, it is probably associated with the movement of dislocations along the planes of the grain boundaries.

Several procedures are available for determining the contribution of grain-boundary sliding to the total strain [116]. This contribution is usually expressed as the ratio $\varepsilon_{gbs}/\varepsilon_t$, where ε_{gbs} is the strain due to grain-

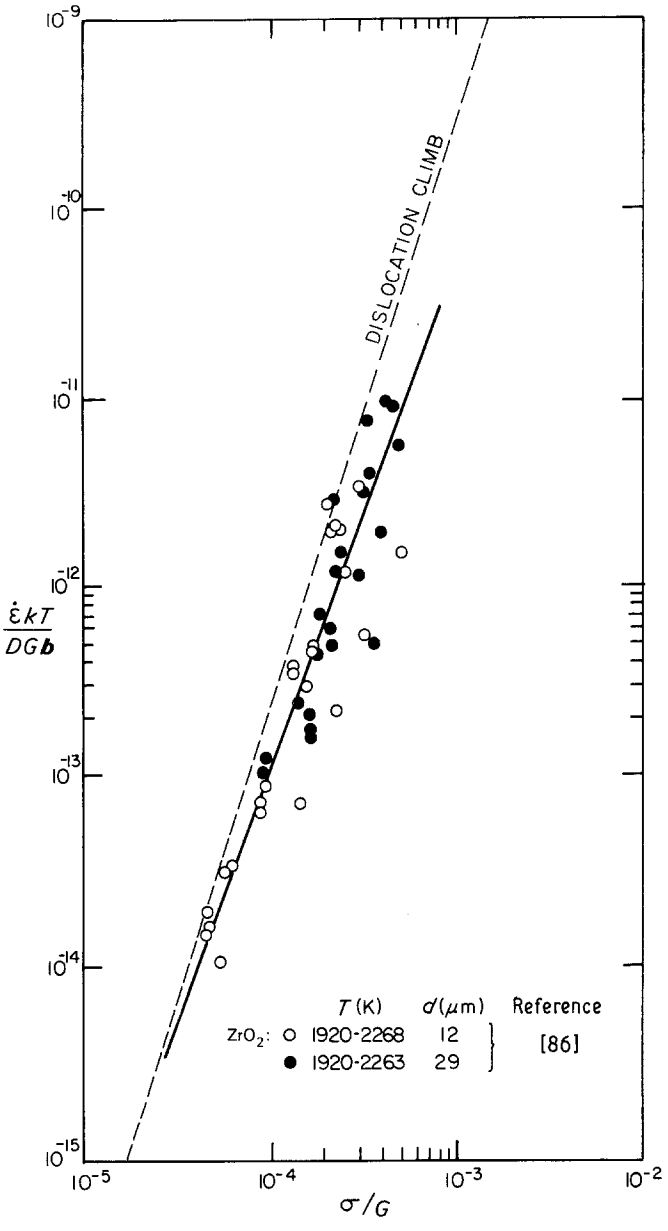

Figure 9 Normalized creep rate plotted against normalized stress for power-law creep in ZrO_2 containing 10% Y_2O_3 [86].

boundary sliding and ε_t is the total strain. An analysis of published data for metals shows that the magnitude of $\varepsilon_{gbs}/\varepsilon_t$ tends to increase with decreasing stress and/or decreasing grain size [117].

Unfortunately, there are very few published measurements of $\varepsilon_{gbs}/\varepsilon_t$ in polycrystalline ceramics, and some investigations have used measuring procedures which are known to be unacceptable. For example, measurements on MgO [118] and a U–Pu carbide [119] were based on a grain-shape procedure which tends to overestimate the values of $\varepsilon_{gbs}/\varepsilon_t$ (this overestimation is confirmed by the reports of values of $\varepsilon_{gbs}/\varepsilon_t$ of 100% and 80 to 100% for MgO [118] and the U–Pu carbide [119], respectively) and measurements on $CaCO_3$ were performed after testing at constant strain rate rather than constant stress [120].

Only two sets of measurements on ceramics were performed using the accepted standard procedures, and these data are summarized in Fig. 13 for Al_2O_3 [52] and MgO [121], respectively. Although very few results are available, the data confirm that, as in metals, sliding increases in importance at the lower stress levels and also with a decrease in grain size.

5. A comparison of creep behaviour in ceramics and metals

As already noted, there are many similarities between the creep behaviour of ceramics and metals. When the grain size is small, as in Figs 1 to 4, the stress exponent is 1 and there is reasonable agreement with the predictions of Nabarro–Herring diffusion creep. At larger grain sizes, there is often a power-law behaviour with a stress exponent of either ~ 5 (Figs 5 and 6) or ~ 3 (Figs 7 to 9).

Figs 14 and 15 show direct comparisons between ceramics and metals for the two groups of ceramics where the values of n are 5 and 3, respectively; the broad hatched areas for ceramics are based on the experimental data documented in Figs 5 to 9, and the broad hatched areas for metals are based on the detailed compilations of data for nominally pure fcc metals and metallic binary solid solution alloys exhibiting $n \simeq 3$, respectively [90].

Fig. 14 shows that the normalized creep rates, $\dot{\varepsilon}kT/DGb$, for ceramics are very similar to, but slightly higher than, the normalized creep rates for pure fcc metals. In fact, as noted by Takeuchi and Argon [122],

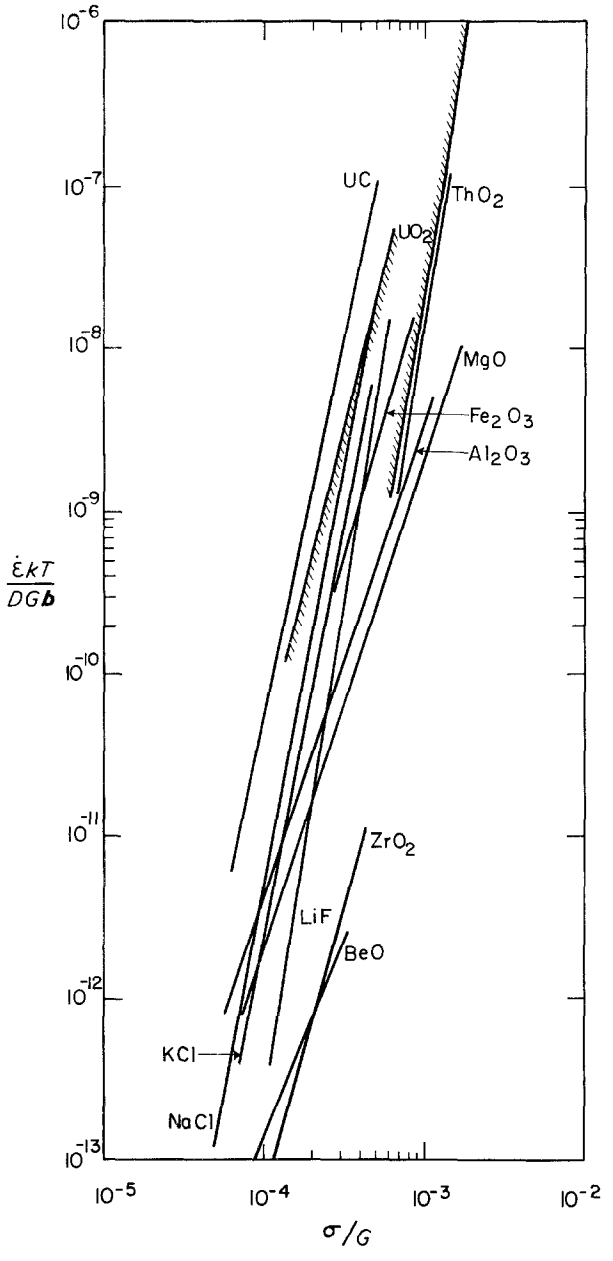

Figure 10 A summary of power-law creep data from Figs 5 to 9.

there are slight differences between the average normalized creep rates for f c c, b c c and h c p metals. The slightly faster creep rates in ceramics may be due to ambipolar diffusion, because the charge separation between the slower and faster ions leads to an enhancement in diffusion of the slower moving species. Under these conditions, the rate of ionic diffusion controlling the creep process is slightly faster than the measured ionic diffusion coefficient.

Although Fig. 15 suggests good agreement between the normalized creep rates of ceramics exhibiting a stress exponent of 3 and metallic solid solution alloys, this agreement is probably fortuitous. As noted earlier, there is excellent agreement in these ceramics between the experimental data and the predictions of the theory for dislocation climb from Bardeen–Herring sources. Furthermore, the experimental observations of subgrain formation in MgO with $n \simeq 3$ [96, 102, 103] are contrary to microstructural observations on metallic solid solution alloys with $n \simeq 3$ where the steady-state substructure consists of an essentially uniform distribution of dislocations without subgrain formation [108].

Figs. 16 and 17 show the substructural parameters, λ/b and $b\varrho^{1/2}$, for ceramics and metals; again, the hatched areas for ceramics are based on the data in Figs 11 and 12 and the metals data are based on the detailed compilation of Bird *et al.* [90].

The agreement between ceramics and metals in Figs 16 and 17 is excellent, and the ceramic data tend to extend the metals data to lower values of the normalized stress, σ/G. The slightly higher values of ζ for ceramics are not significant because of the experimental difficulties of obtaining an accurate measure of the subgrain size, λ.

6. Discussion

6.1. The similarity between ceramics and other materials

There are many similarities between the creep behaviour of ceramics and metals. Both types of material

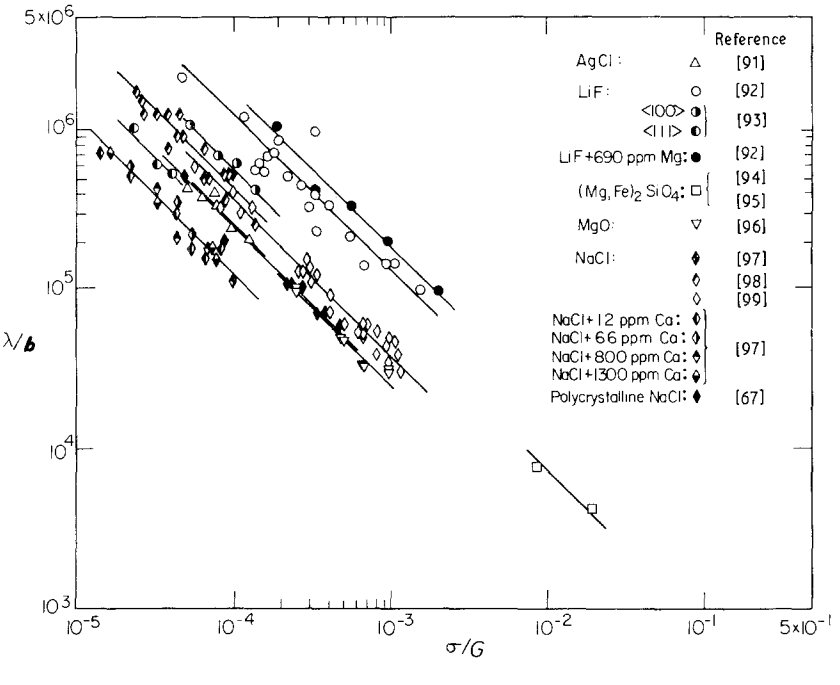

Figure 11 Normalized subgrain size plotted against normalized stress for ceramics [67, 91–99]: each line is drawn through a single set of datum points with a slope of −1.

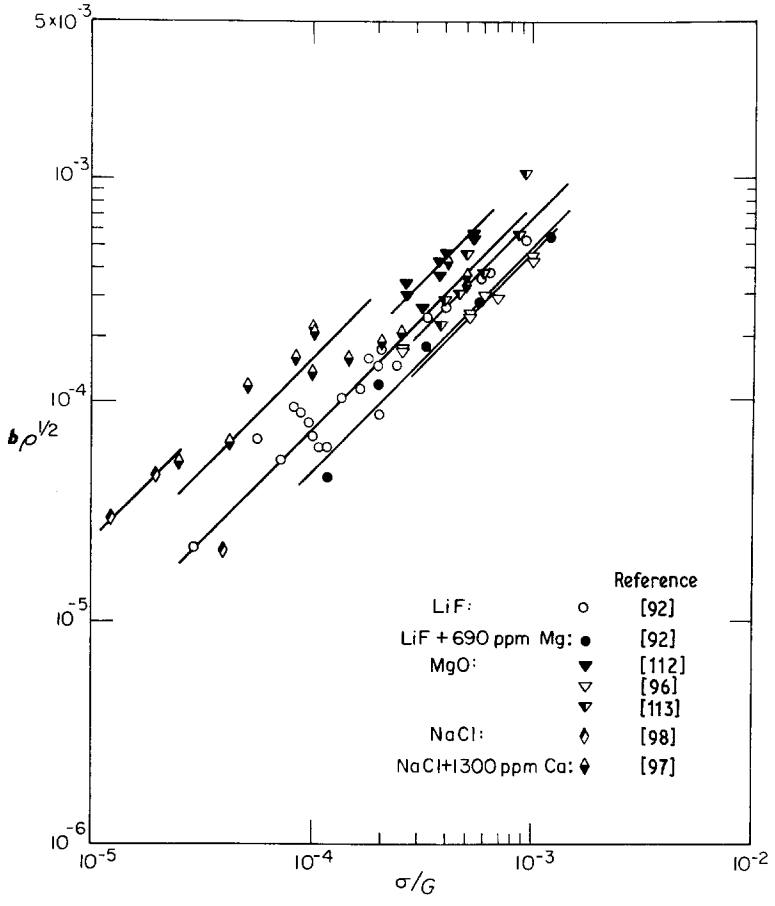

Figure 12 Normalized dislocation density within the subgrains plotted against normalized stress for ceramics; [92, 96–98, 112, 113]: each line is drawn through a single set of datum points with a slope of 1.

exhibit diffusion creep with $n = 1$ at low stresses and some form of dislocation creep with $n \geqslant 3$ at high stresses. In addition, Figs 16 and 17 show that the substructural features are similar in both classes of material.

There are also many similarities between the creep of ceramics and the creep of minerals [123] and it is an accepted procedure to apply the mechanisms of both diffusion creep [124] and dislocation creep [125, 126] to the Earth's mantle. Several minerals show a similar stress exponent close to 3 [127, 128] and with a decrease to an exponent of 1 at the lower stresses [14]. Furthermore, a stress exponent of ~ 3 is observed also in polycrystalline ice [129] and again there is a transition to $n \simeq 1$ at low stress levels [130, 131]. Finally, it should be noted that a transition from $n \simeq 1$ and a dependence on grain size at low stresses to $n > 1$ at high stresses applies also to the densification kinetics during the hot-pressing of ceramic powders (for example, the Al_2O_3–AlN system [132]).

At first sight, it may appear surprising that ceramics exhibit very similar high temperature deformation

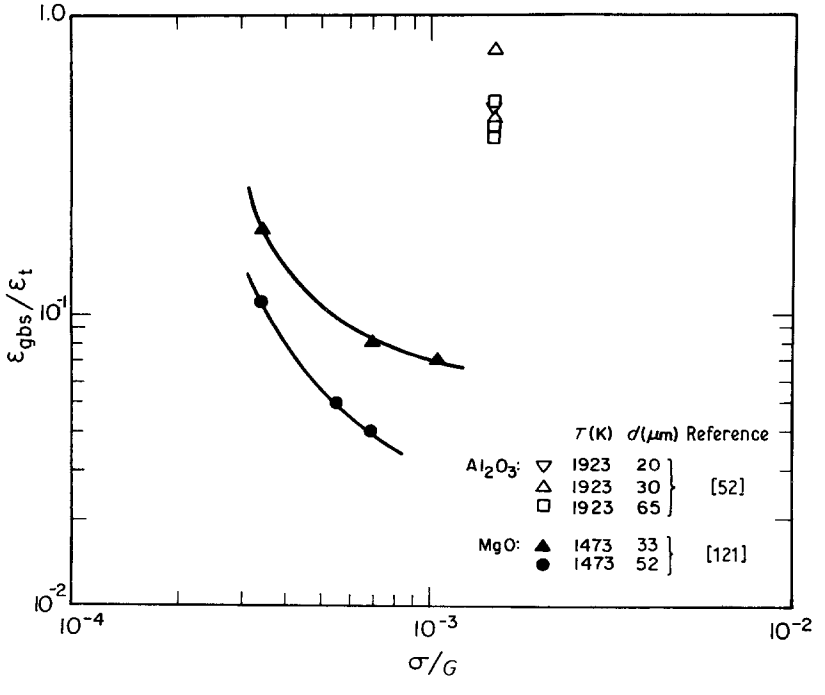

Figure 13 The contribution of grain-boundary sliding to the total strain plotted against normalized stress for Al_2O_3 [52] and MgO [121].

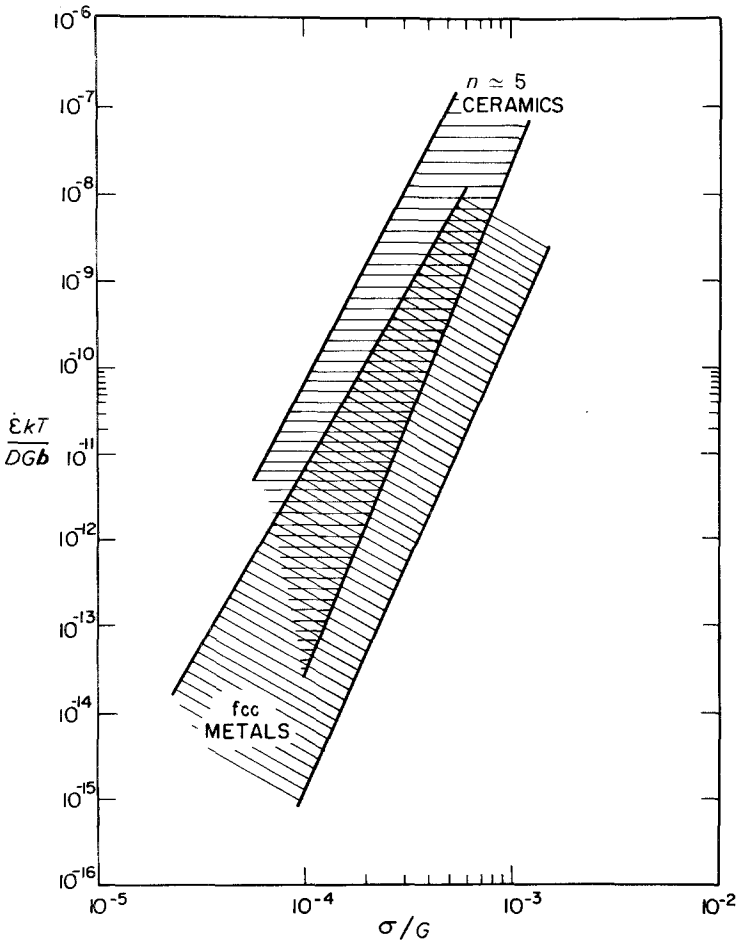

Figure 14 A comparison of the range of experimental creep data for ceramics with $n \simeq 5$ and nominally pure fcc metals, respectively.

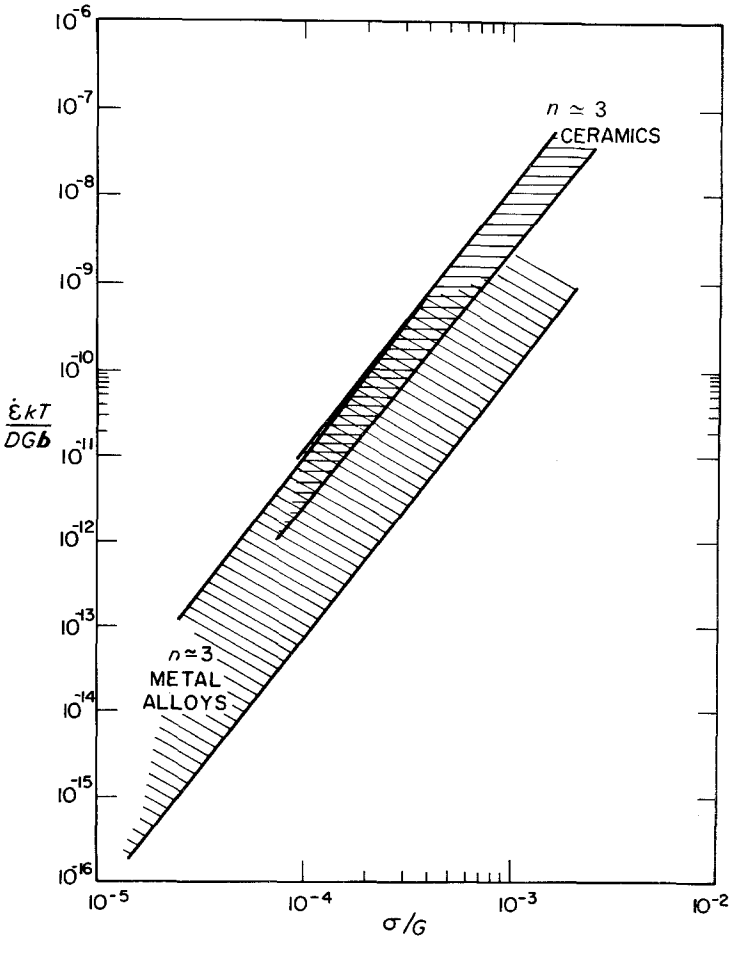

Figure 15 A comparison of the range of experimental creep data for ceramics with $n \simeq 3$ and metallic binary solid solution alloys with $n \simeq 3$, respectively.

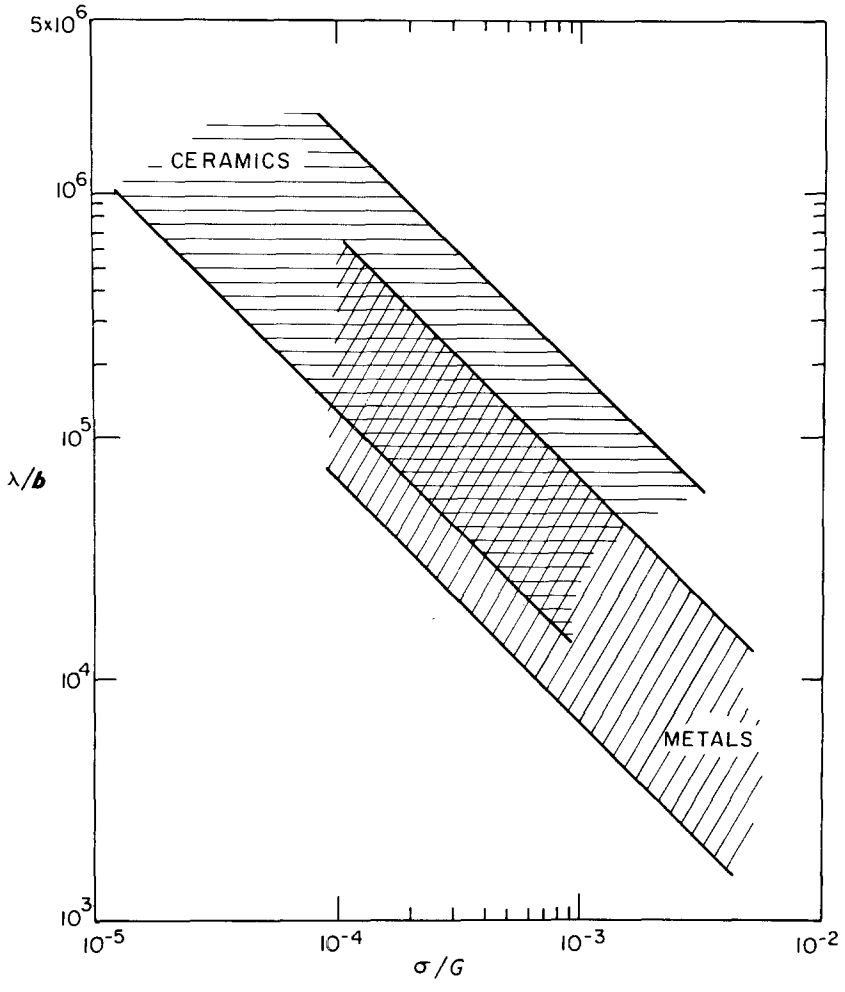

Figure 16 A comparison of the range of normalized subgrain sizes for ceramics and metals.

behaviour to metals, because ceramics have high Peierls forces, low dislocation densities and the possibility of non-active slip systems. However, Fig. 17 shows that the dislocation densities during steady-state creep of ceramics are comparable to those of metals, and, as in metals, the creep of ceramics is a diffusion-controlled process so that the normalized creep rates are fairly similar (Fig. 14).

The diffusion coefficients of crystalline materials are related to the homologous temperature, T/T_m, where T_m is the absolute melting temperature of the material [133, 134], so that the creep rates may be related directly to the homologous testing temperature for both metals and ceramics. Fig. 18 was constructed from the tabulated data of Brown and Ashby [134] and it shows that, at the melting temperature where

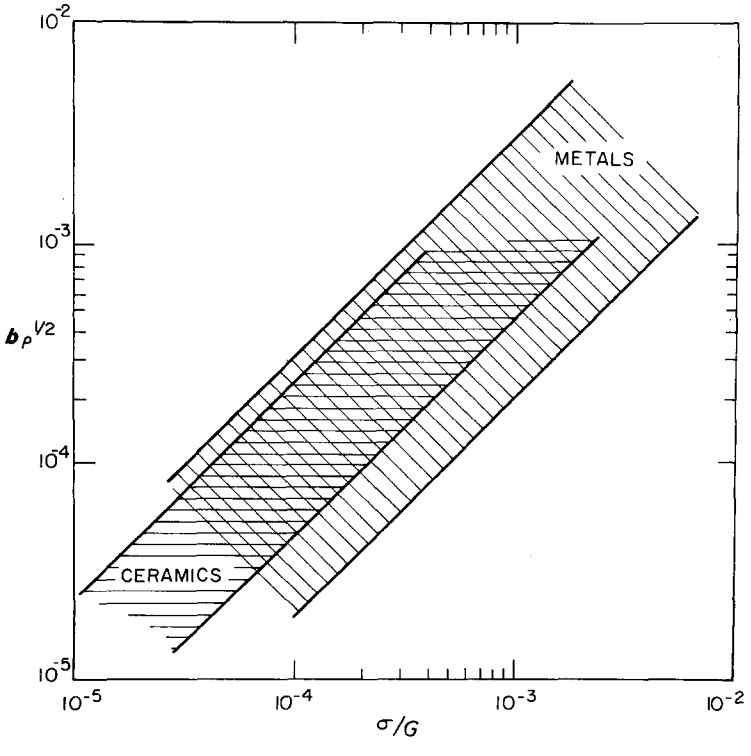

Figure 17 A comparison of the range of normalized dislocation densities within the subgrains for ceramics and metals.

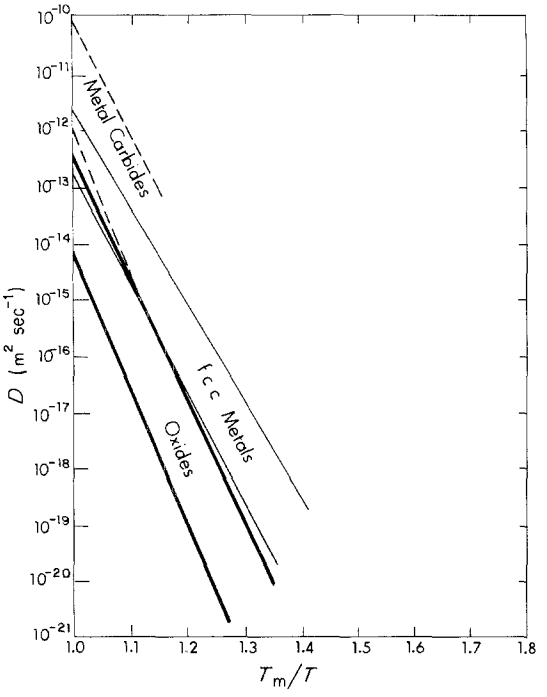

Figure 18 A comparison of diffusion rates in metal carbides, fcc metals and oxides: estimated from the tabulated data of Brown and Ashby [134].

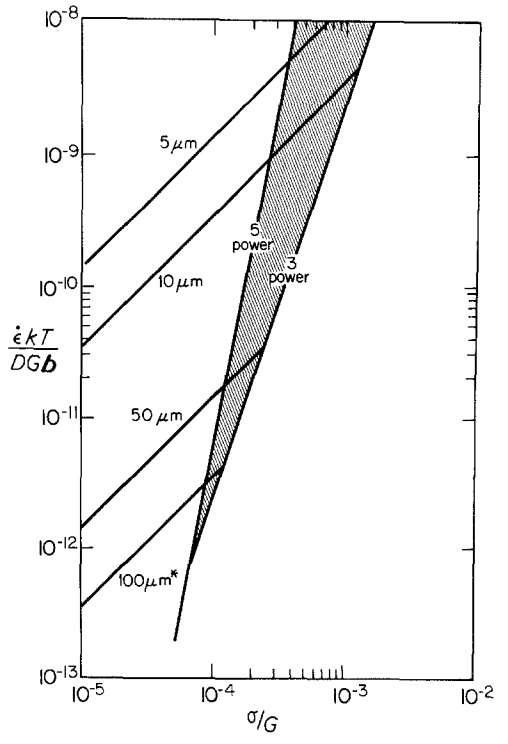

Figure 19 Schematic illustration of normalized creep rate plotted against normalized stress to explain the enhanced role of diffusion creep in ceramics, assuming $D_{cation}/D_{anion} = 10^2$. *1 μm if $D_{cation} = D_{anion}$.

$T_m/T = 1.0$, the intrinsic diffusion rates of the slower moving species in the oxides are about an order of magnitude lower than those of fcc metals. Because the activation energies for diffusion are also generally higher in the oxides than in the fcc metals, it follows that the creep rate of an oxide is lower than that of an fcc metal at a similar homologous temperature.

Despite the overall similarities, there are two major differences between the creep of ceramics and the creep of metals. First, there are relatively few experimental observations of diffusion creep and $n = 1$ in metals whereas this is a common deformation mode in ceramics (Figs 1 to 4). Second, the power-law creep behaviour of ceramics divides into two categories, with stress exponents of ~ 5 and ~ 3, whereas pure metals consistently exhibit stress exponents close to 5. These two differences are examined in the following sections.

6.2. The enhanced role of diffusion creep in ceramics

As documented in Figs 1 to 4 and in Table AIII of Part 1 [1], diffusion creep with $n = 1$ is a common mode of behaviour in ceramics. Under some experimental conditions, the advent of concurrent grain growth precludes the possibility of establishing a true steady-state behaviour at low stresses [135], but in many experiments it has been possible to conclusively establish a stress exponent very close to 1. When experiments are conducted over a wide range of stress, there is also a clear transition to $n > 1$ at the higher stress levels [136].

The enhanced role of diffusion creep in ceramics is often attributed to the high Peierls force or the lack of sufficient slip systems for homogeneous plastic deformation. Inspection shows, however, that these reasons are incorrect. Instead, the prevalence of diffusion creep arises because of two factors which are illustrated in Fig. 19 in a schematic plot of normalized creep rate, $\dot{\varepsilon}kT/DG\boldsymbol{b}$, against normalized stress, σ/G.

First, it is important to recognize that the grain-boundary mobilities in ceramics are lower than in metals so that it is easier to stabilize, and maintain, a very fine grain structure. Whereas most metals (and especially pure metals) have grain sizes of 100 μm or larger, many ceramics have stable grain sizes of the order of 10 μm (Figs 1 to 4). As indicated in Fig. 19, diffusion creep with $n = 1$ extends to higher values of σ/G when the grain size is reduced, and at the same time the creep rates also become faster and more amenable to experimental measurement. The stress range of diffusion creep is further extended in ceramics such as Al_2O_3 and MgO where $n \simeq 3$ at high stresses instead of $n \simeq 5$; using the trends in Figs 14 and 15, the hatched area in Fig. 19 indicates the extra range of stress available for diffusion creep when $n \simeq 3$ in the power-law region.

Second, diffusion creep becomes important in many ceramics because of the preferential enhancement of diffusion of one of the ionic species along the grain boundaries. As noted in Section 3, the faster lattice diffusion coefficient for the cation usually dominates in diffusion creep whereas the slower lattice diffusion coefficient for the anion is usually dominant when the stress exponent is 3 or 5. Assuming a reasonable value of $D_{cation}/D_{anion} = 10^2$, Fig. 19 shows that diffusion creep dominates in a ceramic material with a grain size of 100 μm up to a normalized stress of $\sigma/G \simeq 10^{-4}$, and smaller grain sizes extend diffusion creep to even higher stresses. However, if $D_{cation} = D_{anion}$, which is equivalent to a metal with a single diffusing species, the transition takes place at $\sigma/G \simeq 10^{-4}$ with a grain

size of only 1 μm so that the meaningful stress range for diffusion creep is very much reduced.

It is possible to estimate the upper limiting value of σ/G associated with diffusion creep controlled by cation lattice diffusion by equating $\dot{\varepsilon}$ in Equation 4 with $\dot{\varepsilon}$ in Equations 13 and 17 for $n = 5$ and $n = 3$, respectively. For materials exhibiting $n = 5$ the upper limit is given by

$$\frac{\sigma}{G} = \frac{1.7bM^{0.14}}{d^{0.57}}\left(\frac{D_{\text{cation}}}{D_{\text{anion}}}\right)^{0.29} \quad (20)$$

and for materials exhibiting $n = 3$ the upper limit is

$$\frac{\sigma}{G} = 6.5\left(\frac{b}{d}\right)\left(\frac{D_{\text{cation}}}{D_{\text{anion}}}\right)^{0.5} \quad (21)$$

6.3. The significance of the stress exponents of ~5 and ~3 in ceramics

In the power-law regime of creep, ceramic materials divide into two categories with stress exponents close to 5 and 3, respectively. The behaviour with $n \simeq 5$ is very similar to pure fcc metals, as noted in Fig. 14. However, the behaviour with $n \simeq 3$ cannot be interpreted in terms of a solute drag process, as in metallic solid solution alloys where $n \simeq 3$, for three reasons: (i) there is generally little or no solute, (ii) there are observations of subgrain formation in MgO with $n \simeq 3$ [96, 102, 103] although this is inconsistent with the viscous drag mechanism, and (iii) unlike metallic solid solutions [137], there is no experimental evidence for a transition from $n \simeq 3$ to $n \simeq 5$ with decreasing stress due to the sequential nature of the viscous glide and climb processes. It is therefore necessary to examine more closely the significance of the $n \simeq 3$ behaviour.

It was noted earlier [72] that the ratio of the anion to cation radius, $r_{\text{anion}}/r_{\text{cation}}$, appears to be important, such that ceramics with $n \simeq 3$ have $r_{\text{anion}}/r_{\text{cation}} > 2$ and ceramics with $n \simeq 5$ have $r_{\text{anion}}/r_{\text{cation}} < 2$. Because this ratio is related to the polarizability of the material, it leads to the more general conclusion that $n \simeq 3$ behaviour is associated with either a lack of five independent slip systems and general inhomogeneous plastic deformation or, if five independent slip systems are available, a lack of interpenetration of these systems. Thus, it is concluded, as noted by Wilshire and co-workers [138, 139], that $n \simeq 5$ is associated with fully ductile behaviour and $n \simeq 3$ is associated with plastic creep deformation in a less ductile condition.

A final problem concerns the precise mechanism of flow in ceramics when $n \simeq 3$.

As noted in Fig. 7, there is excellent agreement between the experimental data for Al_2O_3 single crystals with a 0° orientation and the prediction of Equation 17 for dislocation climb from Bardeen–Herring sources. Because these crystals were tested under conditions where there was no basal or prismatic slip, and because there was also no experimental evidence for pyramidal slip, this agreement provides strong support for this creep mechanism.

The situation for the polycrystalline materials is less clearly defined, although for some materials, such as BeO, CVD-SiC and ZrO_2, there is very close agreement between the experimental data and the theoretical prediction. The datum points for polycrystalline Al_2O_3 are scattered above the theoretical line, as shown in Fig. 7, and this may be due to the differences in the impurity levels of the various materials or to the advent of a different creep mechanism.

Evans and Knowles [140] developed a creep mechanism based on the climb of dislocation links in a three-dimensional model, where strain is produced by glide of the edge dislocations. This mechanism contrasts with Equation 16 and the climb of dislocations from Bardeen–Herring sources where it is assumed that climb contributes exclusively to the creep strain. This mechanism leads to a strain rate which is similar to Equation 16 but almost two orders of magnitude faster. Subsequently, Evans and Knowles [141] showed that this mechanism provides reasonable agreement with experimental data on Al_2O_3 but it overestimates the creep rates in MgO. Evans and Knowles [141] also compared their creep mechanism with experimental data for LiF and UO_2 but, as noted in Figs 5 and 6, these materials exhibit $n \simeq 5$ behaviour. These conclusions are consistent with Figs 7 and 8 when it is noted that the datum points for Al_2O_3 are more widely displaced from the theoretical line for dislocation climb. It follows also from Figs 8 and 9 that this creep mechanism is not consistent with the experimental data for BeO, CVD-SiC or ZrO_2.

Based on this analysis, and especially the excellent agreement for Al_2O_3 single crystals in 0° orientation, it is concluded that the creep of ceramics exhibiting $n \simeq 3$ is due to the climb of dislocations from Bardeen–Herring sources under conditions where crystallographic slip is restricted. As noted by Groves and Kelly [142], general deformation may take place through the operation of Bardeen–Herring sources when only a limited number of slip systems is available. The slightly higher creep rates observed in some polycrystalline ceramics may be due to differences in impurity levels and/or they may be due to additional contributions from other creep processes such as restricted slip or the occurrence of grain-boundary sliding. In MgO, for example, some of the specimens documented in Fig. 8 show sliding contributions of the order of 10%, as shown in Fig. 13, and this leads to an enhancement of the overall creep rate.

Finally, it should be noted that the stress exponent of ~5 in pure polycrystalline NaCl and KCl is reduced to ~3 in solid solution alloys having compositions in the range from NaCl–27 mol % KCl to KCl–16.8 mol % NaCl [76]. For these alloys, the observation of $n \simeq 3$ is probably due to a true viscous drag process, as in metallic solid solutions, and calculations indicate a consistency with the criterion developed to predict viscous glide behaviour in metals [143].

7. Conclusions

Part 2 may be summarized briefly as follows:

1. There are many similarities between the creep of ceramics and metals. These similarities include diffusion creep with a stress exponent of $n = 1$ at low stresses, power-law creep with $n \geqslant 3$ at high stresses, an inverse relationship between the subgrain size and the applied stress, σ, a dislocation density within the

subgrains varying with σ^2, and a contribution from grain-boundary sliding which increases with a decrease in stress and/or grain size.

2. The two major differences in the creep of ceramics are (i) the enhanced role of diffusion creep and (ii) the division of creep behaviour into two categories in power-law creep with stress exponents of ~ 5 and ~ 3, respectively. The behaviour with $n \simeq 5$ is interpreted as fully ductile behaviour as in pure f c c metals, and the behaviour with $n \simeq 3$ is interpreted as dislocation climb from Bardeen–Herring sources under conditions where there is either a lack of five independent slip systems and general inhomogeneous deformation or, if five independent slip systems are available, a lack of interpenetration of these systems.

Acknowledgements

This work was supported in part by the United States Department of Energy under contract DE-AM03-76SF00113 PA-DE-AT03-76ER10408 and in part by the National Science Foundation under Grant No. EAR-8518376.

References

1. W. R. CANNON and T. G. LANGDON, *J. Mater. Sci.* **18** (1983) 1.
2. F. R. N. NABARRO, "Report of a Conference on Strength of Solids" (The Physical Society, London, 1948) p. 75.
3. C. HERRING, *J. Appl. Phys.* **21** (1950) 437.
4. G. B. GIBBS, *Mém. Sci. Rev. Mét.* **62** (1965) 781.
5. R. L. COBLE, *J. Appl. Phys.* **34** (1963) 1679.
6. R. S. GORDON, *J. Amer. Ceram. Soc.* **56** (1973) 147.
7. R. S. GORDON, "Mass Transport Phenomena in Ceramics", edited by A. R. Cooper and A. H. Heuer (Plenum, New York, 1975) p. 445.
8. A. G. EVANS and T. G. LANGDON, *Prog. Mater. Sci.* **21** (1976) 171.
9. J. HARPER and J. E. DORN, *Acta Metall.* **5** (1957) 654.
10. P. YAVARI, D. A. MILLER and T. G. LANGDON, *ibid.* **30** (1982) 871.
11. T. G. LANGDON and P. YAVARI, *ibid.* **30** (1982) 881.
12. J. P. HIRTH and J. LOTHE, "Theory of Dislocations" (McGraw-Hill, New York, 1968).
13. J.-P. POIRIER, J. PEYRONNEAU, I. Y. GESLAND and G. BREBEC, *Phys. Earth Planet. Int.* **32** (1983) 273.
14. W. B. BANERDT and C. G. SAMMIS, *ibid.* **41** (1985) 108.
15. P. J. DIXON-STUBBS and B. WILSHIRE, *Philos. Mag. A* **45** (1982) 519.
16. T. G. LANGDON, *ibid.* **47** (1983) L29.
17. A. E. PALADINO and R. L. COBLE, *J. Amer. Ceram. Soc.* **46** (1963) 133.
18. Y. OISHI and W. D. KINGERY, *J. Chem. Phys.* **33** (1960) 480.
19. D. H. CHUNG and G. SIMMONS, *J. Appl. Phys.* **39** (1968) 5316.
20. A. E. PALADINO and W. D. KINGERY, *J. Chem. Phys.* **37** (1962) 957.
21. Y. OISHI and W. D. KINGERY, *ibid.* **33** (1960) 905.
22. N. SOGA and O. L. ANDERSON, *J. Amer. Ceram. Soc.* **49** (1966) 355.
23. R. LINDNER and G. D. PARFITT, *J. Chem. Phys.* **26** (1957) 182.
24. J. B. HOLT, *J. Nucl. Mater.* **11** (1964) 107.
25. R. E. FRYXELL and B. A. CHANDLER, *J. Amer. Ceram. Soc.* **47** (1964) 283.
26. S. B. AUSTERMAN, *J. Nucl. Mater.* **14** (1964) 248.
27. J. D. HONG, R. F. DAVIS and D. E. NEWBURY, *J. Mater Sci.* **16** (1981) 2485.
28. J. B. WACHTMAN and D. G. LAM, *J. Amer. Ceram. Soc.* **42** (1959) 254.
29. M. H. HON, R. F. DAVIS and D. E. NEWBURY, *J. Mater. Sci.* **15** (1980) 2073.
30. K. KIJIMA AND S. SHIRASAKI, *J. Chem. Phys.* **65** (1976) 2668.
31. D. C. LARSEN and J. W. ADAMS, "Property Screening and Evaluation of Ceramic Turbine Materials", Semiannual Report No. 8, June 1980, USAF Contract F33615-C-5100, pp. 22, 55.
32. D. K. REIMANN and T. S. LUNDY, *J. Amer. Ceram. Soc.* **52** (1969) 511.
33. M. O. MARLOWE, *J. Nucl. Mater.* **33** (1969) 242.
34. R. J. HAWKINS and C. B. ALCOCK, *ibid.* **26** (1968) 112.
35. S. SPINNER, F. P. KNUDSEN and L. STONE, *J. Res. Natl Bur. Stds* **67C** (1963) 39.
36. S. SPINNER, L. STONE and F. P. KNUDSEN, *ibid.* **67C** (1963) 93.
37. J. F. LAURENT and J. BÉNARD, *J. Phys. Chem. Solids* **7** (1958) 218.
38. S. HART, *J. Phys. D* **1** (1968) 1285.
39. M. EISENSTADT, *Phys. Rev.* **132** (1963) 630.
40. P. VILLAINE, *Diffusion Data* **3** (1968) 515.
41. A. PADEL and CH. de NOVION, *J. Nucl. Mater.* **33** (1969) 40.
42. W. C. HAGEL, *Trans. AIME* **236** (1966) 179.
43. R. C. LIEBERMANN and E. SCHREIBER, *J. Geophys. Res.* **73** (1968) 6585.
44. O. L. ANDERSON, E. SCHREIBER, R. C. LIEBERMANN and N. SOGA, *Rev. Geophys.* **6** (1968) 491.
45. W. H. RHODES and R. E. CARTER, *J. Amer. Ceram. Soc.* **49** (1966) 244.
46. N. G. PACE, G. A. SAUNDERS, Z. SUEMEUGEN and J. S. THORP, *J. Mater. Sci.* **4** (1969) 1106.
47. A. CROSBY and P. E. EVANS, *ibid.* **8** (1973) 1573.
48. A. H. HEUER, R. M. CANNON and N. J. TIGHE, "Ultra Fine-Grain Ceramics", edited by J. J. Burke, N. L. Reed and V. Weiss (Syracuse University Press, Syracuse, New York, 1970) p. 339.
49. P. A. LESSING and R. S. GORDON, "Deformation of Ceramic Materials", edited by R. C. Bradt and R. E. Tressler (Plenum, New York, 1975) p. 271.
50. R. C. FOLWEILER, *J. Appl. Phys.* **32** (1961) 773.
51. C. K. L. DAVIES, "Physical Metallurgy of Reactor Fuel Elements", edited by J. E. Harris and E. C. Sykes (The Metals Society, London, 1975) p. 99.
52. W. R. CANNON and O. D. SHERBY, *J. Amer. Ceram. Soc.* **60** (1977) 44.
53. R. T. TREMPER, PhD dissertation, University of Utah (1971).
54. R. R. VANDERVOORT and W. L. BARMORE, *J. Amer. Ceram. Soc.* **43** (1963) 180.
55. W. L. BARMORE and R. R. VANDERVOORT, *ibid.* **48** (1965) 499.
56. R. F. DAVIS, personal communication (1985).
57. M. S. SELTZER, *Bull. Amer. Ceram. Soc.* **56** (1977) 418.
58. L. E. POTEAT and C. S. YUST, "Ceramic Microstructures," edited by R. M. Fulrath and J. A. Pask (Wiley, New York, 1968) p. 646.
59. P. E. BOHABOY, R. R. ASAMOTO and A. E. CONTI, Rprt. No. GEAP-10054 (General Electric Breeder Reactor Development Operation, Sunnyvale, California, 1969).
60. J. A. C. MARPLES and A. HOUGH, "Plutonium 1970 and Other Actinides", edited by W. N. Miner (The Metallurgical Society of AIME, New York, 1970) p. 479.
61. M. S. SELTZER, A. H. CLAUER and B. A. WILCOX, *J. Nucl. Mater.* **34** (1970) 351.
62. *Idem, ibid.* **44** (1972) 331.
63. B. BURTON and G. L. REYNOLDS, *Acta Metall.* **21** (1973) 1641.
64. J. WEERTMAN, *J. Appl. Phys.* **28** (1957) 362.
65. P. M. HAZZLEDINE, *Can. J. Phys.* **45** (1967) 765.
66. J. WEERTMAN, "Rate Processes in Plastic Deformation of Materials", edited by J. C. M. Li and A. K. Mukherjee (American Society for Metals, Metals Park, Ohio, 1975) p. 315.

67. P. M. BURKE, PhD dissertation, Stanford University (1968).
68. O. D. SHERBY and P. M. BURKE, *Prog. Mater. Sci.* **13** (1968) 325.
69. J. WEERTMAN, *J. Appl. Phys.* **28** (1957) 1185.
70. F. A. MOHAMED and T. G. LANGDON, *Acta Metall.* **22** (1974) 779.
71. S. TAKEUCHI and A. S. ARGON, *ibid.* **24** (1976) 883.
72. W. R. CANNON and O. D. SHERBY, *J. Amer. Ceram. Soc.* **56** (1973) 157.
73. F. R. N. NABARRO, *Philos. Mag.* **16** (1967) 231.
74. J. WEERTMAN, *Trans. ASM* **61** (1968) 681.
75. D. R. CROPPER and T. G. LANGDON, *Philos. Mag.* **18** (1968) 1181.
76. W. R. CANNON and O. D. SHERBY, *J. Amer. Ceram. Soc.* **53** (1970) 346.
77. M. S. SELTZER, T. R. WRIGHT and D. P. MOAK, *ibid.* **58** (1975) 138.
78. C. H. CARTER, R. F. DAVIS and J. BENTLEY, *ibid.* **67** (1984) 409.
79. S. I. WARSHAW and F. H. NORTON, *ibid.* **45** (1962) 479.
80. G. ENGELHARDT and F. THÜMMLER, *Ber. Deut. Keram. Ges.* **47** (1970) 571.
81. A. G. CROUCH, *J. Amer. Ceram. Soc.* **55** (1972) 558.
82. J. H. HENSLER and G. V. CULLEN, *ibid.* **51** (1968) 178.
83. T. G. LANGDON and J. A. PASK, *Acta Metall.* **18** (1970) 505.
84. W. L. BARMORE and R. R. VANDERVOORT, *J. Amer. Ceram. Soc.* **50** (1967) 316.
85. C. H. CARTER, R. F. DAVIS and J. BENTLEY, *ibid.* **67** (1984) 732.
86. M. S. SELTZER and P. K. TALTY, *ibid.* **58** (1975) 124.
87. F. A. MOHAMED and T. G. LANGDON, *J. Appl. Phys.* **45** (1974) 1965.
88. R. F. FIRESTONE and A. H. HEUER, *J. Amer. Ceram. Soc.* **59** (1976) 24.
89. T. G. LANGDON, "Dislocations and Properties of Real Materials" (The Institute of Metals, London, 1985) p. 221.
90. J. E. BIRD, A. K. MUKHERJEE and J. E. DORN, "Quantitative Relation Between Properties and Microstructure," edited by D. G. Brandon and A. Rosen (Israel Universities Press, Jerusalem, 1969) p. 255.
91. V. PONTIKIS and J.-P. POIRIER, *Philos. Mag.* **32** (1975) 577.
92. G. STREB and B. REPPICH, *Phys. Status Solidi (a)* **16** (1973) 493.
93. D. R. CROPPER and J. A. PASK, *Philos. Mag.* **27** (1973) 1105.
94. C. B. RALEIGH and S. H. KIRBY, *Mineral. Soc. Amer. Spec. Pap.* **3** (1970) 113.
95. H. W. GREEN and S. V. RADCLIFFE, "Flow and Fracture of Rocks", edited by H. C. Heard, I. Y. Borg, N. L. Carter and C. B. Raleigh (American Geophysical Union, Washington, DC, 1972) p. 139.
96. W. HÜTHER and B. REPPICH, *Philos. Mag.* **28** (1973) 363.
97. F. SCHUH, W. BLUM and B. ILSCHNER, *Proc. Brit. Ceram. Soc.* **15** (1970) 143.
98. J.-P. POIRIER, *Phil. Mag.* **26** (1972) 701.
99. W. BLUM, personal communication (1976).
100. A. V. STEPANOV and I. M. EIDUS, *J. Exper. Theoret. Phys. USSR* **29** (1955) 669.
101. V. PONTIKIS and J.-P. POIRIER, *Scripta Metall.* **8** (1974) 1427.
102. J. B. BILDE-SÖRENSEN, *Acta Metall.* **21** (1973) 1495.
103. M. HURM and B. ESCAIG, *J. Physique. Colloque. C9* **34** (1973) C9-347.
104. H. W. GREEN and S. V. RADCLIFFE, *Earth Planet. Sci. Lett.* **15** (1972) 239.
105. A. E. RINGWOOD, "Composition and Petrology of the Earth's Mantle" (McGraw-Hill, New York, 1975).
106. W. B. DURHAM, C. GOETZE and B. BLAKE, *J. Geophys. Res.* **82** (1977) 5755.
107. R. J. TWISS, *Pure Appl. Geophys.* **115** (1977) 227.
108. T. G. LANGDON, "Strength of Metals and Alloys (ICSMA 6)", Vol. 3, edited by R. C. Gifkins (Pergamon, Oxford, 1983) p. 1105.
109. J. V. ROSS, H. G. AVÉ LALLEMANT and N. L. CARTER, *Tectonophys.* **70** (1980) 39.
110. A. J. ARDELL, J. M. CHRISTIE and J. A. TULLIS, *Cryst. Lattice Defects* **4** (1973) 275.
111. S. WHITE, *Contrib. Mineral. Petrol.* **70** (1979) 193.
112. J. B. BILDE-SÖRENSEN, *J. Amer. Ceram. Soc.* **55** (1972) 606.
113. A. H. CLAUER and B. A. WILCOX, *ibid.* **59** (1976) 89.
114. D. L. KOHLSTEDT, C. GOETZE and W. B. DURHAM, "The Physics and Chemistry of Minerals and Rocks", edited by R. G. J. Strens (Wiley, London, 1976) p. 35.
115. C. GOETZE and D. L. KOHLSTEDT, *Contrib. Mineral. Petrol.* **59** (1977) 293.
116. T. G. LANGDON, *Met. Trans.* **3** (1972) 797.
117. T. G. LANGDON and R. B. VASTAVA, "Mechanical Testing for Deformation Model Development", edited by R. W. Rohde and J. C. Swearengen (American Society for Testing and Materials, Philadelphia, 1982) STP 765, p. 435.
118. J. H. HENSLER and G. V. CULLEN, *J. Amer. Ceram. Soc.* **50** (1967) 584.
119. M. TOKAR, *ibid.* **56** (1973) 173.
120. H. C. HEARD and C. B. RALEIGH, *Geol. Soc. Amer. Bull.* **83** (1972) 935.
121. T. G. LANGDON, *J. Amer. Ceram. Soc.* **58** (1975) 92.
122. S. TAKEUCHI and A. S. ARGON, *J. Mater. Sci.* **11** (1976) 1542.
123. S. H. KIRBY and C. B. RALEIGH, *Tectonophys.* **19** (1973) 165.
124. R. B. GORDON, *J. Geophys. Res.* **70** (1965) 2413.
125. J. WEERTMAN, *Rev. Geophys. Space Phys.* **8** (1970) 145.
126. *Idem, Phil. Trans. R. Soc. A* **288** (1978) 9.
127. D. L. KOHLSTEDT and C. GOETZE, *J. Geophys. Res.* **79** (1974) 2045.
128. H. TSUKAHARA, *J. Phys. Earth* **22** (1974) 343.
129. J. W. GLEN, *Proc. R. Soc. A* **228** (1955) 519.
130. M. MELLOR and J. H. SMITH, "Physics of Snow and Ice", Vol. 1, Part 2, edited by H. Ôura (Institute of Low Temperature Science, Hokkaido University, Sapporo, Japan, 1967) p. 843.
131. T. G. LANGDON, "Physics and Chemistry of Ice," edited by E. Whalley, S. J. Jones and L. W. Gold (Royal Society of Canada, Ottawa, 1973) p. 356.
132. J.-P. Le COMPTE, J. JARRIGE, J. MEXMAIN, R. J. BROOK and F. L. RILEY, *J. Mater. Sci.* **16** (1981) 3093.
133. O. D. SHERBY and M. T. SIMNAD, *Trans. ASM* **54** (1961) 227.
134. A. M. BROWN and M. F. ASHBY, *Acta Metall.* **28** (1980) 1085.
135. A. H. CHOKSHI and J. R. PORTER, *J. Amer. Ceram. Soc.* **69** (1986) C-37.
136. M. JIMENEZ-MELENDO, J. CABRERA-CAÑO, A. DOMINGUEZ-RODRIGUEZ and J. CASTAING, *J. Physique* **44** (1983) L-339.
137. P. YAVARI, F. A. MOHAMED and T. G. LANGDON, *Acta Metall.* **29** (1981) 1495.
138. B. WILSHIRE and B. WATKINS, *J. Mater. Sci.* **12** (1977) 2135.
139. R. W. EVANS, P. J. SCHARNING and B. WILSHIRE, "Creep Behaviour of Crystalline solids", edited by B. Wilshire and R. W. Evans (Pineridge Press, Swansea, Wales, 1985) p. 201.
140. H. E. EVANS and G. KNOWLES, *Acta Metall.* **25** (1977) 963.
141. *Idem, ibid.* **26** (1978) 141.
142. G. W. GROVES and A. KELLY, *Philos. Mag.* **19** (1969) 977.
143. F. A. MOHAMED and T. G. LANGDON, *J. Amer. Ceram. Soc.* **58** (1975) 533.

Received 14 January
and accepted 19 January 1987